# Broadband Point Source Green's Function in a One-Dimensional Infinite Periodic Lossless Medium Based on BBGFL with Modal Method

**Leung Tsang[1, *], Kung-Hau Ding[2], and Shurun Tan[1]**

**Abstract**—In this paper we calculate Green's function of a single point source in a one-dimensional infinite periodic lossless medium. The method is based on Broadband Green's Functions with Low Wavenumber Extractions (BBGFL) that express the Green's functions in terms of band solutions that are wavenumber independent. The converegnce of the band expansions are accelerated by a low wavenumber extraction with the wavenumber chosen at the mid-bandgap. The choice of mid-bandgap means that the extracted low wavenumber Green's function can be calculated with very few number of layers. The broadband Green's functions are illustrated for stopband, passband and close to the bandedge. For the case of passband and close to band edge, a modal method is used with first order and second order pole extractions, respectively. The modal terms are extracted and integrated analytically. The calculated solutions of single point source Green's functions are compared with the scattering solutions of multilayers using as many as $200,000$ layers for the case of passband and near bandedge. The BBGFL computed solutions are in good agreement with those of scattering solutions for stopband, passband, and close to the bandedge.

## 1. INTRODUCTION

The subject of Green's function is basic knowledge in electromagnetics and is treated in graduate texts [1–5]. The free space Green's functions have been extensively used in the formulation of integral equations which are solved by the method of moments (MoM). For the case of periodic structures, the periodic Green's functions have periodic sources. However, they are that of empty lattice without scatterers. Neither the free space Green's function nor the empty lattice periodic Green's functions satisfy boundary conditions on the scatterers. For the Green's functions that satisfy boundary conditions, there are only a few such as rectangular waveguides, cylindrical waveguides, infinitely long cylinders, spheres, layered media, etc. [1–5].

Recently, we have been developing the broadband Green's functions with low wavenumber extractions (BBGFL) for problems in waveguides and periodic structures [6–17]. We label the usual techniques as the "scattering method". In the scattering method, such as the Multiple Scattering Theory [18], Fast Multipole Method [19], the free space Green's function is used to formulate the scattering problem, using vector spherical waves or MoM [20]. To satisfy boundary conditions on all the scatterers, the multiple scattering solution is calculated. The multiple scattering solution must be calculated every time. The Broadband Green's Method is based on band theory. It is recognized that the band solutions are the multiple scattering solutions and satisfy boundary conditions. A distinct feature of BBGFL is that the Green's functions are expressed in terms of the band solutions. The band

solutions are calculated once. The solution of the Green's function at every frequency is obtained by merely changing the denominator. For the BBGFL technique to work efficiently, three set-up steps are essential. (i) The band solutions, eigenvalues and eigenvectors, are cast in a linear eigenvalue problem of relative small matrix size compared to plane wave expansions. The eigenvalues and the modal field solutions are solved simultaneously. The band field wavenumbers and the band field solutions have to be accurate. (ii) The modal/band field solutions must be normalized efficiently without requiring extensive volumetric integrations, and (iii) the modal summation for Green's function is not convergent and acceleration technique with low wavenumber extraction is to be exercised. It is noted that the setup is only performed once, and then the BBGFL works for all frequencies (up to a maximum frequency), by merely changing the denominator.

For the case of periodic structures, we previously derived the single point source Green's functions [11, 12, 16, 17]. Solutions are computed for the case when the low/small wavenumbers are in the stopband. For the passband, losses are needed to obtain the solutions. The cases when there are only small losses in the passband were not considered.

In this paper, we calculate the Broadband Green's Function of a single point source in a one-dimensional (1D) infinite periodic lossless medium. For the case of a single point source in a 1D medium, the usual method is using scattering solutions. For the case of lossless medium with $\text{Im}(k_0) = 0$, where Im is imaginary part and $k_0$ is the wavenumber, the numerical solutions do not converge. For the ideal lossless case in free space, with field point at $z$ and source point at $z'$, the free space Green's function is $\frac{e^{ik_0|z-z'|}}{2ik_0}$ which assumes radiation boundary condition. An alternative of getting the free space solution is to assume artificial infinitesimal loss. For the case of 1D periodic structure with infinitesimal loss, if the scattering method is used, a very large number of layers is required to obtain the physical solution of infinitesimal loss.

In this paper, we consider the case when the band starting at $k_0 = 0$ is in the passband. Thus it is not feasible to use a small wavenumber extraction as it is not practical to calculate the Green's function for the small wavenumber. In this paper, the wavenumber extraction is chosen at the mid-bandgap $k_g$. The choice of mid-bandgap does not need to be precise. This choice of mid-bandgap means that the extracted solution can be calculated with very few number of layers with the fewest when the wavenumber is in the mid-bandgap. The extraction mid-bandgap wavenumber can be higher than $k_0$ which is in the passband. We still call it the low wavenumber (in the bandgap), as $k_g$ is still lower than the highest wavenumber in the truncated band expansions.

In this paper, the single point source Broadband Green's Functions with Low Wavenumber Extractions (BBGFL) are illustrated for stopband, passband, and close to the band edge, for the lossless (infinitesimal loss) case. We take the liberty to define the lossless case. By lossless case, we first define a maximum distance of interest. Then, 1) within the maximum distance of interest, the Green's function behaves as the medium is lossless (infinitesimal loss), and 2) within the maximum distance, the Green's function is independent of the artificial loss put in the simulations. The calculated solutions of point source Green's functions of lossless media are compared with the scattering solutions for the case of passband and bandedges. The advantage of 1D case is that we can take a large number of layers, such as $200,000$ layers, for the scattering solutions to converge when the wavenumber is near the bandedge. The BBGFL computed solutions are in good agreement with those of scattering solutions for stopband, passband, and close to the bandedge. For the case of passband, we use a modal approach with a first order pole extraction. For the case close to the bandedge, we also apply a modal approach using a second order pole extraction.

The new contributions in this paper are as follows: (i) an improvement of methodology is the choice of a single low wavenumber extraction for the case of point source Green's function rather than low wavenumber extraction for the periodic Green's functions of each Bloch vector, (ii) choice of mid-bandgap solution as the low wavenumber extraction, (iii) use of a modal approach with first and second order pole extractions for the point source Green's functions at passband/bandedge, and (iv) an improvement in normalization showing the accuracies of the band field solutions that are in good agreement with benchmark ABCD method [21]. This paper is a review and making new improvements.

The organization of the paper is as follows. In Section 2, we use BBGFL to compute the band solutions and the normalizations of the band solutions. In Section 3, we describe the computations of the single point source broadband Green's functions for the cases of passband and stopband. In

Section 3, we also describe the second order modal approach for close to the bandedge. In Section 4, numerical results are illustrated.

## 2. BAND EIGENVALUES AND NORMALIZED BAND MODE SOLUTIONS BASED ON BBGFL

In this section, we apply the BBGFL method for the eigenvalue problem of band solutions. Methods used to compute band structures include the plane wave method [22] and the finite element method [23]. The advantages of BBGFL are (i) few terms of plane wave expansions are needed because boundary contributions are added from the low wavenumber extraction, (ii) the eigenvalue problem is linear meaning that the matrix is independent of eigenvalues, and (iii) the normalization of modes require only surface fields rather than volumetric integration.
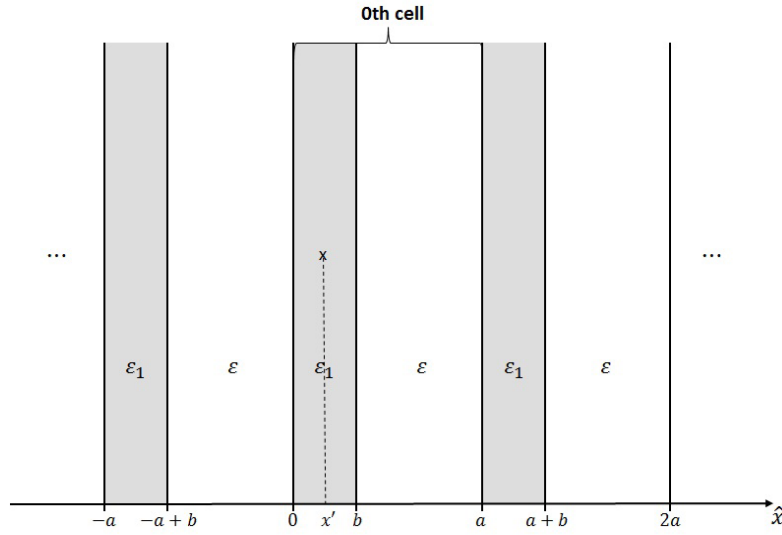


**Figure 1.** An infinite periodic one-dimension medium. Calculation of single point source Green's function $g_{j1}^S(k_0, x, x')$ with single point source at $x' = \frac{b}{2}$.

Consider a one-dimensional periodic structure in Figure 1 with region 1 as the scatterer and region 2 as the background. The period is $a$. The thickness of region 1 is $b$. In the 0-th cell, for $0 \leq x \leq b$, the permittivity and wavenumber are $\varepsilon_1$ and $k_1$, respectively, with $k_1 = \omega\sqrt{\mu_0\varepsilon_1}$, where $\omega$ is the angular frequency and $\mu_0$ is the permeability. We use $\varepsilon_0$ as the free space permittivity and $k_0 = \omega\sqrt{\mu_0\varepsilon_0}$ as the free space wavenumber. In region 2, $b \leq x \leq a$, the permittivity and wavenumber are $\varepsilon_2 = \varepsilon$, and $k_2 = k$, respectively, with $k = \omega\sqrt{\mu_0\varepsilon}$. The wave solutions $\psi$, representing the tangential components of electric fields, are

$$\psi = \begin{cases} \psi_1 & \text{for } 0 \leq x \leq b \\ \psi_2 & \text{for } b \leq x \leq a \end{cases} \tag{1}$$

The band solutions are $\psi_1$ and $\psi_2$, respectively, obey the wave equations

$$\frac{d^2\psi_1}{dx^2} + k_1^2\psi_1 = 0 \tag{2}$$

in region 1, and

$$\frac{d^2\psi_2}{dx^2} + k^2\psi_2 = 0 \tag{3}$$

in region 2. The boundary conditions are the continuities of wave functions and their derivatives at the interface $x = 0$ and at $x = b$. At $x = 0$ and $x = b$,

$$\psi_1 = \psi_2 \tag{4}$$

$$\frac{d\psi_1}{dx} = \frac{d\psi_2}{dx} \tag{5}$$

Let $k_i$ be the Bloch wave vector, then the wave functions satisfy the Bloch wave condition.

$$\psi(x + a) = e^{ik_i a}\psi(x) \tag{6}$$

The Bloch wave functions can be written as

$$\psi(x) = e^{ik_i x}u(x) \tag{7}$$

where $u(x)$ is a periodic function of period $a$.

The band solutions can be obtained by the ABCD method [21] and plane wave method [22, 24]. We apply the BBGFL method using surface integral equations and periodic Green's functions of empty lattice of period $a$. For the case of empty lattice with wavenumber $k_1$ and the periodic source at $x'$, $0 \le x' \le b$, the periodic sources are at $x' + na$ and $n$ is an integer. In spectral domain, the periodic Green's functions of empty lattice $g_{jP}^0(k_0, k_i; x, x')$, $j = 1$ or $2$, can be expressed as

$$g_{jP}^0\left(k_0, k_i; x, x'\right) = \frac{1}{a}\sum_\alpha \frac{1}{k_{i\alpha}^2 - k_j^2}e^{ik_{i\alpha}(x-x')} \tag{8}$$

In Equation (8), the subscript "$P$" stands for periodic, and the superscript "0" stands for empty space, $k_j^2 = k_0^2\frac{\varepsilon_j}{\varepsilon_0}$, and

$$k_{i\alpha} = k_i + \alpha\frac{2\pi}{a} \tag{9}$$

with $\alpha$ being an integer, $\alpha = 0, \pm1, \pm2, \dots$. Note that $g_{jP}^0$ depends on $x - x'$. In spatial domain, $g_{jP}^0(k_0, k_i; x)$, $j = 1$ or $2$, becomes

$$g_{jP}^0\left(k_0, k_i; x\right) = \sum_n \frac{i}{2k_j}e^{ik_i na}e^{ik_j|x-na|} \tag{10}$$

The geometric series can be summed so that, for $0 \le x < a$,

$$g_{jP}^0\left(k_0, k_i; x\right) = \frac{i}{2k_j}\left[e^{ik_j x}\frac{1}{1 - e^{i(k_j - k_i)a}} + e^{-ik_j x}\frac{e^{i(k_j + k_i)a}}{1 - e^{i(k_j + k_i)a}}\right] \tag{11}$$

The $g_{jP}^0$ obeys the Bloch condition so that

$$g_{jP}^0\left(k_0, k_i; x + a\right) = e^{ik_i a}g_{jP}^0\left(k_0, k_i; x\right) \tag{12}$$

Using the periodic conditions, we can calculate $g_{jP}^0(k_0, k_i; 0^-)$ and $g_{jP}^{0\prime}(k_0, k_i; 0^-)$ etc., where prime stands for derivative with respect to $x$.

For the case of empty lattice with wavenumber $k_j$ and with periodic sources at $x'$, the empty lattice periodic Green's function is

$$g_{jP}^0\left(k_0, k_i; x, x'\right) = \sum_n \frac{i}{2k_j}e^{ik_i na}e^{ik_j|x-(x'+na)|} \tag{13}$$

Note that the Green's functions derivatives have discontinuities at $x = x' + na$.

## 2.1. Band Eigenvalue Problem

The eigenvalue problem is derived in a manner similar to the two-dimensional (2D) case in [9]. Applying Green's theorem and using both Green's functions of wavenumbers $k_1$ and $k$ yields the extinction theorem. The derivations of Eqs. (14) and (15) are given in Appendix A.

$$-\left[\psi_1\left(x'\right)\frac{d}{dx'}g_{1P}^0\left(k_0, k_i; x, x'\right) - \frac{d\psi_1\left(x'\right)}{dx'}g_{1P}^0\left(k_0, k_i; x, x'\right)\right]\Bigg|_{x'=0^+}^{|x'=b^-} = \begin{cases} \psi_1(x) & 0 < x < b \\ 0 & b < x < a \end{cases} \tag{14}$$

$$\left[\psi_1\left(x'\right)\frac{d}{dx'}g_{2P}^0\left(k_0, k_i; x, x'\right) - \frac{d\psi_1\left(x'\right)}{dx}g_{2P}^0\left(k_0, k_i; x, x'\right)\right]\Bigg|_{x'=0^-}^{|x'=b^+} = \begin{cases} 0 & 0 < x < b \\ \psi_2(x) & b < x < a \end{cases} \tag{15}$$

The surface integral equations are obtained by taking $x \to 0^-$ and $b^+$ in Eq. (14), and taking $x \to 0^+$ and $b^-$ in Eq. (15), where the superscripts $+$ and $-$ represent approaching a point from its right and left, respectively. The surface integral equations can be readily put in matrix form as

$$\left[ \begin{array}{cc} \bar{\bar{S}}_1(k_0) & -\bar{\bar{L}}_1(k_0) \\ \bar{\bar{S}}_2(k_0) & -\bar{\bar{L}}_2(k_0) \end{array} \right] \left[ \begin{array}{c} \bar{p} \\ \bar{q} \end{array} \right] = 0 \tag{16}$$

where the unknowns $\bar{p}$ and $\bar{q}$ are the boundary values of $\psi_1$ and $\psi_1'$ at $x = 0$ and $x = b$,

$$\bar{p} = \left[ \begin{array}{c} -\psi_1(0) \\ \psi_1(b) \end{array} \right] \tag{17}$$

$$\bar{q} = \left[ \begin{array}{c} -\psi_1'(0) \\ \psi_1'(b) \end{array} \right] \tag{18}$$

and $\bar{\bar{S}}_1(k_0)$, $\bar{\bar{L}}_1(k_0)$, $\bar{\bar{S}}_2(k_0)$, and $\bar{\bar{L}}_2(k_0)$ are the impedance matrices.

$$\bar{\bar{S}}_1(k_0) = \left[ \begin{array}{cc} \dfrac{d}{dx'} g_{1P}^0(k_0, k_i; 0^-, 0^+) & \dfrac{d}{dx'} g_{1P}^0(k_0, k_i; 0^-, b^-) \\ \dfrac{d}{dx'} g_{1P}^0(k_0, k_i; b^+, 0^+) & \dfrac{d}{dx'} g_{1P}^0(k_0, k_i; b^+, b^-) \end{array} \right] \tag{19}$$

$$\bar{\bar{L}}_1(k_0) = \left[ \begin{array}{cc} g_{1P}^0(k_0, k_i; 0^-, 0^+) & g_{1P}^0(k_0, k_i; 0^-, b^-) \\ g_{1P}^0(k_0, k_i; b^+, 0^+) & g_{1P}^0(k_0, k_i; b^+, b^-) \end{array} \right] \tag{20}$$

$$\bar{\bar{S}}_2(k_0) = \left[ \begin{array}{cc} \dfrac{d}{dx'} g_{2P}^0(k_0, k_i; 0^+, 0^-) & \dfrac{d}{dx'} g_{2P}^0(k_0, k_i; 0^+, b^+) \\ \dfrac{d}{dx'} g_{2P}^0(k_0, k_i; b^-, 0^-) & \dfrac{d}{dx'} g_{2P}^0(k_0, k_i; b^-, b^+) \end{array} \right] \tag{21}$$

$$\bar{\bar{L}}_2(k_0) = \left[ \begin{array}{cc} g_{2P}^0(k_0, k_i; 0^+, 0^-) & g_{2P}^0(k_0, k_i; 0^+, b^+) \\ g_{2P}^0(k_0, k_i; b^-, 0^-) & g_{2P}^0(k_0, k_i; b^-, b^+) \end{array} \right] \tag{22}$$

Setting the determinant of Eq. (16) equal to zero gives a nonlinear eigenvalue problem for $k_0$, the band solution. The nonlinear eigenvalue refers to the fact that the matrix on the left hand side of Eq. (16) is dependent on $k_0$. To convert it to a linear eigenvalue problem, we use low wavenumber extractions on the periodic Green's functions. Let $g_{jP}^0(k_{0L}, k_i; x, x')$ be a single low wavenumber solution at $k_0 = k_{0L}$. Then the extracted form gives

$$g_{jP}^0(k_0, k_i; x, x') - g_{jP}^0(k_{0L}, k_i; x, x') = \frac{1}{a} \sum_\alpha \frac{\dfrac{\varepsilon_j}{\varepsilon_0}(k_0^2 - k_{0L}^2)}{\left(k_{i\alpha}^2 - \dfrac{\varepsilon_j}{\varepsilon_0}k_0^2\right)\left(k_{i\alpha}^2 - \dfrac{\varepsilon_j}{\varepsilon_0}k_{0L}^2\right)} e^{ik_{i\alpha}(x-x')}$$

$$= \frac{1}{a} \sum_\alpha \left[ \frac{1}{\dfrac{1}{\dfrac{\varepsilon_j}{\varepsilon_0}(k_0^2 - k_{0L}^2)} - \dfrac{1}{(k_{i\alpha})^2 - \dfrac{\varepsilon_j}{\varepsilon_0}k_{0L}^2}} \right] \frac{e^{ik_{i\alpha}(x-x')}}{\left[(k_{i\alpha})^2 - \dfrac{\varepsilon_j}{\varepsilon_0}k_{0L}^2\right]^2} \tag{23}$$

Note that after extraction, the plane wave expansion converges as $1/k_{i\alpha}^4$ which has a higher order convergence than $1/k_{i\alpha}^2$ of the original spectral summation in Eq. (8). Eq. (23) can be put in the following form,

$$g_{jP}^0(k_0, k_i; x, x') = g_{jP}^0(k_{0L}, k_i; x, x') + \sum_\alpha R_\alpha^{(j)}(k_{0L}, x) W_\alpha^{(j)} R_\alpha^{(j)}(k_{0L}, -x') \tag{24}$$

where

$$R_\alpha^{(j)}(k_{0L}, x) = \frac{1}{\sqrt{a}} \frac{e^{ik_{i\alpha}x}}{k_{i\alpha}^2 - \frac{\varepsilon_j}{\varepsilon_0}k_{0L}^2} = D_\alpha^{(j)} \psi_\alpha^0(x) \tag{25}$$

and

$$\psi_\alpha^0(x) = \frac{1}{\sqrt{a}} e^{ik_{i\alpha}x} \tag{26}$$

$$\lambda(k_0, k_{0L}) = \frac{1}{k_0^2 - k_{0L}^2} \tag{27}$$

$$D_\alpha^{(j)}(k_{0L}) = \frac{1}{k_{i\alpha}^2 - \dfrac{\varepsilon_j}{\varepsilon_0} k_{0L}^2} \tag{28}$$

$$W_\alpha^{(j)}(k_0, k_{0L}) = \frac{1}{\dfrac{\varepsilon_0}{\varepsilon_j}\lambda - D_\alpha^{(j)}} \tag{29}$$

Note that after the singularity is extracted in the low wavenumber term, $g_{jP}^0(k_{0L}, k_i; x, x')$, the plane wave summation term of $\sum_\alpha$ does not have singularity at any $x$. We put the eigen-equations in matrix form. Let there be $M$ plane waves used in Eq. (24) with $M$ being an odd number. Then, $N = \frac{M-1}{2}$ is an integer. Thus the plane wave index $\alpha$ has $M$ values with $\alpha = 0 \pm 1, \pm 2, \ldots, \pm N$. Because of the low wavenumber extraction, using Eq. (24) in impedance matrices $\bar{\bar{S}}$ and $\bar{\bar{L}}$, we have

$$\bar{\bar{S}}_1(k_0) = \bar{\bar{S}}_1(k_{0L}) + \bar{\bar{R}}_1(k_{0L})\bar{\bar{W}}_1(k_0, k_{0L})\bar{\bar{Q}}_1(k_{0L}) \tag{30}$$

$$\bar{\bar{L}}_1(k_0) = \bar{\bar{L}}_1(k_{0L}) + \bar{\bar{R}}_1(k_{0L})\bar{\bar{W}}_1(k_0, k_{0L})\bar{\bar{T}}_1(k_{0L}) \tag{31}$$

$$\bar{\bar{S}}_2(k_0) = \bar{\bar{S}}_2(k_{0L}) + \bar{\bar{R}}_2(k_{0L})\bar{\bar{W}}_2(k_0, k_{0L})\bar{\bar{Q}}_2(k_{0L}) \tag{32}$$

$$\bar{\bar{L}}_2(k_0) = \bar{\bar{L}}_2(k_{0L}) + \bar{\bar{R}}_2(k_{0L})\bar{\bar{W}}_2(k_0, k_{0L})\bar{\bar{T}}_2(k_{0L}) \tag{33}$$

where $\bar{\bar{R}}$, $2 \times M$, $\bar{\bar{D}}$, $M \times M$, $\bar{\bar{W}}$, $M \times M$, $\bar{\bar{Q}}$, $M \times 2$, and $\bar{\bar{T}}$, $M \times 2$ are matrices defined in Appendix B.

Notice that the dimensions of matrices $\bar{\bar{S}}_1$, $\bar{\bar{L}}_1$, $\bar{\bar{S}}_2$, and $\bar{\bar{L}}_2$ are $2 \times 2$. Then the governing matrix Eq. (16) becomes

$$\bar{\bar{S}}_1(k_{0L}) - \bar{\bar{L}}_1(k_{0L})\bar{q} + \bar{\bar{R}}_1(k_{0L})\bar{\bar{W}}_1(k_0, k_{0L})\bar{\bar{Q}}_1(k_{0L})\bar{p} - \bar{\bar{R}}_1(k_{0L})\bar{\bar{W}}_1(k_0, k_{0L})\bar{\bar{T}}_1(k_{0L})\bar{q} = 0 \tag{34}$$

$$\bar{\bar{S}}_2(k_{0L}) - \bar{\bar{L}}_2(k_{0L})\bar{q} + \bar{\bar{R}}_2(k_{0L})\bar{\bar{W}}_2(k_0, k_{0L})\bar{\bar{Q}}_2(k_{0L})\bar{p} - \bar{\bar{R}}_2(k_{0L})\bar{\bar{W}}_2(k_0, k_{0L})\bar{\bar{T}}_2(k_{0L})\bar{q} = 0 \tag{35}$$

which are analogous to Eqs. (14a) and (14b) of reference [8]. Let

$$\bar{c}_j = \bar{\bar{W}}_j(k_0, k_{0L})\bar{\bar{Q}}_j(k_{0L})\bar{p} - \bar{\bar{W}}_j(k_0, k_{0L})\bar{\bar{T}}_j(k_{0L})\bar{q} \tag{36}$$

where $\bar{c}_j$ are vectors of dimension $M \times 1$. Using

$$\left[\bar{\bar{W}}_j(k_0, k_{0L})\right]^{-1} = \frac{\varepsilon_0}{\varepsilon_j}\lambda\bar{\bar{I}}_M - \bar{\bar{D}}_j \tag{37}$$

we have

$$\lambda\bar{c}_j = \frac{\varepsilon_j}{\varepsilon_0}\left[\bar{\bar{D}}_j\bar{c}_j + \bar{\bar{Q}}_j(k_{0L})\bar{p} - \bar{\bar{T}}_j(k_{0L})\bar{q}\right] \tag{38}$$

where $\bar{\bar{I}}_M$ is an $M \times M$ unit matrix.

Substituting Eq. (36) into Eqs. (34) and (35), and expressing $\bar{p}$ and $\bar{q}$ in terms of $\bar{c}_j$, we readily obtain

$$\begin{bmatrix} \bar{p} \\ \bar{q} \end{bmatrix} = \bar{\bar{A}}(k_{0L})\begin{bmatrix} \bar{c}_1 \\ \bar{c}_2 \end{bmatrix} \tag{39}$$

where

$$\bar{\bar{A}}(k_{0L}) = -\begin{bmatrix} \bar{\bar{S}}_1(k_{0L}) & -\bar{\bar{L}}_1(k_{0L}) \\ \bar{\bar{S}}_2(k_{0L}) & -\bar{\bar{L}}_2(k_{0L}) \end{bmatrix}^{-1}\begin{bmatrix} \bar{\bar{R}}_1(k_{0L}) & \bar{\bar{0}}_{2M} \\ \bar{\bar{0}}_{2M} & \bar{\bar{R}}_2(k_{0L}) \end{bmatrix} \tag{40}$$

with $\bar{\bar{0}}_{2M}$ being a zero matrix of dimension $2 \times M$. Substitution of Eq. (39) into Eq. (36) gives the eigenvalue equation

$$\bar{\bar{P}}\begin{bmatrix} \bar{c}_1 \\ \bar{c}_2 \end{bmatrix} = \lambda\begin{bmatrix} \bar{c}_1 \\ \bar{c}_2 \end{bmatrix} \tag{41}$$

where

$$\bar{\bar{P}} = \begin{bmatrix} \frac{\varepsilon_1}{\varepsilon_0}\bar{\bar{D}}_1 & \bar{\bar{0}}_M \\ \bar{\bar{0}}_M & \frac{\varepsilon}{\varepsilon_0}\bar{\bar{D}}_2 \end{bmatrix} + \begin{bmatrix} \frac{\varepsilon_1}{\varepsilon_0}\bar{\bar{Q}}_1 & -\frac{\varepsilon_1}{\varepsilon_0}\bar{\bar{T}}_1 \\ \frac{\varepsilon_2}{\varepsilon_0}\bar{\bar{Q}}_2 & -\frac{\varepsilon_2}{\varepsilon_0}\bar{\bar{T}}_2 \end{bmatrix} \bar{\bar{A}} \tag{42}$$

with $\bar{\bar{0}}_M$ being a zero matrix of dimension $M \times M$. The eigenvalues $\lambda$'s are as defined in Eq. (27). The eigenvalue problem is linear because the matrix $\bar{\bar{P}}$ is independent of wavenumber $k_0$. The matrix $\bar{\bar{P}}$ depends on the low wavenumber $k_{0L}$ and $k_{i\alpha}$. The eigenvalue problem is of dimension $2M$, much smaller than using purely plane wave bases.

## 2.2. Band Field Solution and Normalization

We describe the band field solution and its normalization. Note that the band field solution from BBGFL is a "hybrid" representation consisting of a sum of surface terms and plane wave terms. In the numerical results section, we show that the surface terms eliminate the Gibbs phenomena which exist when only plane waves basis are used.

The extinction theorems in Eqs. (14) and (15) imply that we can extend the domain of definition of $\psi_1$ and $\psi_2$ to the entire period with $0 < x < a$. The advantages of extinction theorem are that $\psi_1$ and $\psi_2$ vanishes outside its validity domain, respectively. Then the modal field $\psi(x)$ can be expressed as

$$\psi(x) = \psi_1(x) + \psi_2(x) \tag{43}$$

The modal band solutions are related to the band eigenvectors, $\bar{c}_1$ and $\bar{c}_2$, and the band solutions of surface currents, $\bar{p}$ and $\bar{q}$, where Eq. (39) represents the surface currents in terms of the eigenvectors. Using the BBGFL representation of $g_{1P}$ and $g_{2P}$, we obtain band field eigensolutions from the extinction theorems. Let

$$\bar{\bar{S}}_0^{(1)}(k_{0L}, x) = \begin{bmatrix} \frac{d}{dx'}g_{1P}(k_{0L}; x, 0^+) & \frac{d}{dx'}g_{1P}(k_{0L}; x, b^-) \end{bmatrix} \tag{44}$$

$$\bar{\bar{L}}_0^{(1)}(k_{0L}, x) = \begin{bmatrix} g_{1P}(k_{0L}; x, 0^+) & g_{1P}(k_{0L}; x, b^-) \end{bmatrix} \tag{45}$$

$$\bar{\bar{S}}_0^{(2)}(k_{0L}, x) = \begin{bmatrix} \frac{d}{dx'}g_{2P}(k_{0L}; x, 0^-) & \frac{d}{dx'}g_{2P}(k_{0L}; x, b^+) \end{bmatrix} \tag{46}$$

$$\bar{\bar{L}}_0^{(2)}(k_{0L}, x) = \begin{bmatrix} g_{2P}(k_{0L}; x, 0^-) & g_{2P}(k_{0L}; x, b^+) \end{bmatrix} \tag{47}$$

and $\psi_\alpha^0(x) = \frac{1}{\sqrt{a}}e^{ik_{i\alpha}x}$ are the normalized Floquet plane waves as defined in Eq. (26). The unnormalized band field solutions are

$$\psi_1(x) = -\begin{bmatrix} \bar{\bar{S}}_0^{(1)}(k_{0L}, x) & -\bar{\bar{L}}_0^{(1)}(k_{0L}, x) \end{bmatrix}\begin{bmatrix} \bar{p} \\ \bar{q} \end{bmatrix} - \sum_{|\alpha|\leq N} \psi_\alpha^0(x) D_\alpha^{(1)} c_\alpha^{(1)} \tag{48}$$

$$\bar{\psi}_2(x) = \begin{bmatrix} \bar{\bar{S}}_0^{(2)}(k_{0L}, x) & -\bar{\bar{L}}_0^{(2)}(k_{0L}, x) \end{bmatrix}\begin{bmatrix} \bar{p} \\ \bar{q} \end{bmatrix} + \sum_{|\alpha|\leq N} \psi_\alpha^0(x) D_\alpha^{(2)} c_\alpha^{(2)} \tag{49}$$

Note that the band field solutions in Eqs. (48) and (49) above have two contributions: one from the boundary terms and one from the plane wave summations. The plane wave summation is $N = \frac{M-1}{2}$ which is a relatively small number of plane wave modes as the surface terms have been extracted to accelerate convergence. The boundary contributions are evaluated at a single $k_{0L}$ to accurately account for the low wavenumber contributions. As shown in the numerical results section, this term removes the Gibbs oscillations arising from truncating the series in Eq. (53) and significantly improves the accuracy in evaluating the modal fields. In the following, we describe the improvement that is made in the accuracy of band normalization in this paper.

Note that we only have $c_\alpha^{(j)}$, for $|\alpha| \leq N$, in the linear eigenvalue problem. We set $c_\alpha^{(j)} = 0$ for $|\alpha| > N$. We define the normalized field as $\widetilde{\psi}(x)$ which is related to $\psi(x)$ through a normalization

coefficient $E$.

$$\widetilde{\psi}(x) = E\psi(x) \tag{50}$$

The normalization condition of the band field solution can be derived using differential equations, Eqs. (2)–(3), and boundary conditions, Eqs. (4)–(5).

$$\frac{\varepsilon_1}{\varepsilon_0} \int_0^b dx \widetilde{\psi}_1(x) \widetilde{\psi}_1^*(x) + \frac{\varepsilon}{\varepsilon_0} \int_b^a dx \widetilde{\psi}_2(x) \widetilde{\psi}_2^*(x) = 1 \tag{51}$$

Using the extended domain of definitions of $\psi_1$ and $\psi_2$ from the extinction theorem, we extend the domain of integration to 0 to $a$, and readily obtain

$$|E|^2 = \frac{1}{\dfrac{\varepsilon_1}{\varepsilon_0} \displaystyle\int_0^a dx\psi_1(x)\psi_1^*(x) + \dfrac{\varepsilon}{\varepsilon_0} \displaystyle\int_0^a dx\psi_2(x)\psi_2^*(x)} \tag{52}$$

In order to evaluate the integrals without computing $\psi_1(x)$ and $\psi_2(x)$ everywhere, we expand $\psi_1(x)$ and $\psi_2(x)$ into plane waves,

$$\psi_j(x) = \sum_\alpha \psi_\alpha^0(x) b_\alpha^{(j)} \tag{53}$$

with $j = 1, 2$. We then truncate the plane wave expansion series using the same number of terms as used in the BBGFL and a remainder.

$$\psi_j(x) = \sum_{|\alpha| \leq N} \psi_\alpha^0(x) b_\alpha^{(j)} + h^{(j)}(x) \tag{54}$$

where $h^{(j)}(x)$ is the remainder of using a truncated plane wave series to approximate $\psi_j(x)$.

$$h^{(j)}(x) = \sum_{|\alpha| > N} \psi_\alpha^0(x) b_\alpha^{(j)} \tag{55}$$

Note that $b_\alpha^{(j)}$ are not the same as $D_\alpha^{(j)} c_\alpha^{(j)}$ because the boundary terms have been included. Truncating the series creates Gibbs oscillations, while the remainder $h^{(j)}(x)$ eliminates the Gibbs oscillations.

From the orthogonality of $\psi_\alpha^0(x)$, we have

$$\left\langle h^{(j)}(x), \sum_{|\alpha| \leq N} \psi_\alpha^0(x) b_\alpha^{(j)} \right\rangle = \int_0^a dx h^{(j)*}(x) \sum_{|\alpha| \leq N} \psi_\alpha^0(x) b_\alpha^{(j)} = 0 \tag{56}$$

and

$$\int_0^a dx\psi_j(x)\psi_j^*(x) = \sum_{|\alpha| \leq N} \left| b_\alpha^{(j)} \right|^2 + \int_0^a dx \left| h^{(j)}(x) \right|^2 \tag{57}$$

The orthogonality of $\psi_\alpha^0(x)$ also indicates

$$b_\alpha^{(j)} = \int_0^a dx\psi_\alpha^{0*}(x)\psi^{(j)}(x) \tag{58}$$

To evaluate the coefficients $b_\alpha$'s, we make use of plane wave expansion of $g_{1P}$ and $g_{2P}$ in Eqs. (48) and (49)

$$g_{jP}\left(k_{0L}.\bar{k}_i; x, x'\right) = \sum_\alpha \psi_\alpha^0(x)\psi_\alpha^0(-x') D_\alpha^{(j)} \tag{59}$$

$$\frac{d}{dx'} g_{jP}\left(k_{0L}.\bar{k}_i; x, x'\right) = \sum_\alpha \psi_\alpha^0(x)(-ik_{i\alpha})\psi_\alpha^0(-x') D_\alpha^{(j)} \tag{60}$$

and readily obtain, from the orthogonality of $\psi_\alpha^0(x)$,

$$b_\alpha^{(1)} = -D_\alpha^{(1)}\left[\widetilde{c}_\alpha + c_\alpha^{(1)}\right] \tag{61}$$

$$b_\alpha^{(2)} = D_\alpha^{(2)}\left[\widetilde{c}_\alpha + c_\alpha^{(2)}\right] \tag{62}$$

where

$$\widetilde{c}_\alpha = \left[ \begin{array}{cccc} (-ik_{i\alpha})\,\psi_\alpha^0\,(0) & (-ik_{i\alpha})\,\psi_\alpha^0\,(-b) & -\psi_\alpha^0\,(0) & -\psi_\alpha^0\,(-b) \end{array} \right] \left[ \begin{array}{c} \bar{p} \\ \bar{q} \end{array} \right] \tag{63}$$

Thus $\widetilde{c}_\alpha$ represents the addition from the boundary terms to the plane wave expansions. To evaluate $\int_0^a dx |h^{(j)}(x)|^2$, the second term in Eq. (57), we first derive $h^{(j)}(x)$ from the following equation.

$$h^{(j)}(x) = \psi_j(x) - \sum_{|\alpha| \leq N} \psi_\alpha^0(x)\, b_\alpha^{(j)} \tag{64}$$

Substitution of $\psi_j(x)$ in Eqs. (48) and (49), and the expression of $b_\alpha^{(j)}$ in Eqs. (61) and (62), leads to

$$h^{(1)}(x) = -\left[ \begin{array}{cccc} \dfrac{d}{dx'} g_{1P}\left(k_{0L}; x, 0^+\right) & \dfrac{d}{dx'} g_{1P}\left(k_{0L}; x, b^-\right) & -g_{1P}\left(k_{0L}; x, 0^+\right) & -g_{1P}\left(k_{0L}; x, b^-\right) \end{array} \right] \left[ \begin{array}{c} \bar{p} \\ \bar{q} \end{array} \right]$$
$$+ \sum_{|\alpha| \leq N} \psi_\alpha^0(x)\, D_\alpha^{(1)} \widetilde{c}_\alpha \tag{65}$$

and

$$h^{(2)}(x) = \left[ \begin{array}{cccc} \dfrac{dg_{2P}^{(0)}\left(k_{0L}, k_i, x, 0^-\right)}{dx'} & \dfrac{dg_{2P}^{(0)}\left(k_{0L}, k_i, x, b^+\right)}{dx'} & -g_{2P}^{(0)}\left(k_{0L}, k_i; x, 0^-\right) & -g_{2P}^{(0)}\left(k_{0L}, k_i; x, b^+\right) \end{array} \right] \left[ \begin{array}{c} \bar{p} \\ \bar{q} \end{array} \right]$$
$$- \sum_{|\alpha| \leq N} \psi_\alpha^0(x)\, D_\alpha^{(2)} \widetilde{c}_\alpha \tag{66}$$

Thus $h^{(1)}(x)$ and $h^{(2)}(x)$ are the remainders after subtracting, from the boundary terms, contributions from $\sum_{|\alpha| \leq N}$.

Using the above we can numerically evaluate $\int_0^a dx |h^{(j)}(x)|^2$. The normalization is then

$$|E|^2 = \frac{1}{\displaystyle\sum_j \frac{\varepsilon_j}{\varepsilon_0} \left[ \displaystyle\sum_{|\alpha| \leq N} \left| b_\alpha^{(j)} \right|^2 + \int_0^a dx \left| h^{(j)}(x) \right|^2 \right]} \tag{67}$$

Eqs. (65)–(66) can be expressed more explicitly using Eq. (63).

$$h^{(1)}(x) = -\left[ \begin{array}{cccc} h_1^{(1)}(x) & h_2^{(1)}(x) & -h_3^{(1)}(x) & -h_4^{(1)}(x) \end{array} \right] \left[ \begin{array}{c} \bar{p} \\ \bar{q} \end{array} \right] \tag{68}$$

$$h^{(2)}(x) = \left[ \begin{array}{cccc} h_1^{(2)}(x) & h_2^{(2)}(x) & -h_3^{(2)}(x) & -h_4^{(2)}(x) \end{array} \right] \left[ \begin{array}{c} \bar{p} \\ \bar{q} \end{array} \right] \tag{69}$$

where

$$h_1^{(j)}(x) = \frac{d}{dx'} g_{jP}\left(k_{0L}; x, 0\right) - \sum_{|\alpha| \leq N} \psi_\alpha^0(x)\, D_\alpha^{(j)}\left(-ik_{i\alpha}\right) \psi_\alpha^0(0) \tag{70}$$

$$h_2^{(j)}(x) = \frac{d}{dx'} g_{jP}\left(k_{0L}; x, b\right) - \sum_{|\alpha| \leq N} \psi_\alpha^0(x)\, D_\alpha^{(j)}\left(-ik_{i\alpha}\right) \psi_\alpha^0(-b) \tag{71}$$

$$h_3^{(j)}(x) = g_{jP}\left(k_{0L}; x, 0\right) - \sum_{|\alpha| \leq N} \psi_\alpha^0(x)\, D_\alpha^{(j)} \psi_\alpha^0(0) \tag{72}$$

$$h_4^{(j)}(x) = g_{jP}\left(k_{0L}; x, b\right) - \sum_{|\alpha| \leq N} \psi_\alpha^0(x)\, D_\alpha^{(j)} \psi_\alpha^0(-b) \tag{73}$$

We can put the reminder in plane wave expansions. Eqs. (70)–(73) become, respectively,

$$h_1^{(j)}(x) = \sum_{|\alpha| > N} \psi_\alpha^0(x)\, D_\alpha^{(j)}\left(-ik_{i\alpha}\right) \psi_\alpha^0(0) = \sum_{|\alpha| > N} \psi_\alpha^0(x)\, h_{1\alpha}^{(j)} \tag{74}$$

$$h_2^{(j)}(x) = \sum_{|\alpha|>N} \psi_\alpha^0(x) D_\alpha^{(j)}(-ik_{i\alpha}) \psi_\alpha^0(-b) = \sum_{|\alpha|>N} \psi_\alpha^0(x) h_{2\alpha}^{(j)} \tag{75}$$

$$h_3^{(j)}(x) = \sum_{|\alpha|>N} \psi_\alpha^0(x) D_\alpha^{(j)}\psi_\alpha^0(0) = \sum_{|\alpha|>N} \psi_\alpha^0(x) h_{3\alpha}^{(j)} \tag{76}$$

$$h_4^{(j)}(x) = \sum_{|\alpha|>N} \psi_\alpha^0(x) D_\alpha^{(j)}\psi_\alpha^0(-b) = \sum_{|\alpha|>N} \psi_\alpha^0(x) h_{4\alpha}^{(j)} \tag{77}$$

where $h_{1\alpha}^{(j)}$, $h_{2\alpha}^{(j)}$, $h_{3\alpha}^{(j)}$, and $h_{4\alpha}^{(j)}$ are the plane wave expansion coefficients defined accordingly.

Using Eqs. (68) and (69) in $\int_0^a dx|h^{(j)}(x)|^2$ leads to

$$\int_0^a dx \left|h^{(j)}(x)\right|^2 = \left[\begin{array}{c}\bar{p}\\\bar{q}\end{array}\right]^\dagger \bar{\bar{H}}^{(j)} \left[\begin{array}{c}\bar{p}\\\bar{q}\end{array}\right] \tag{78}$$

where $\bar{\bar{H}}^{(j)}$ is a 4 by 4 matrix, and its component, $H_{st}^{(j)}$, is related to $\int_0^a dx h_s^{(j)*}(x)h_t^{(j)}(x)$ with the proper sign. Putting together yields

$$|E|^2 = \cfrac{1}{\displaystyle\sum_j \frac{\varepsilon_j}{\varepsilon_0}\left[\sum_{|\alpha|\leq N}\left|b_\alpha^{(j)}\right|^2 + \left[\begin{array}{c}\bar{p}\\\bar{q}\end{array}\right]^\dagger \bar{\bar{H}}^{(j)}\left[\begin{array}{c}\bar{p}\\\bar{q}\end{array}\right]\right]} \tag{79}$$

Volumetric integrations are not required in Eq. (79). After the normalization coefficient $E$ is computed from Eq. (79), we go back to Eqs. (48) and (49) to evaluate the band fields. Both set of Eqs. (70)–(73) and (74)–(77) work for the 1D case. This continues to be a subject of investigation for the 2D and 3D case. The goal is to avoid volumetric integration for normalization of band solutions which can be computational intensive if one needs to do volumetric integration for every band solution.

# 3. SINGLE POINT SOURCE GREEN'S FUNCTION $g^S(k_0, x, x')$

In this section, we derive the Green's function for a single point source $g^S(k, x, x')$ in the infinite periodic medium. We consider the single point source at $x'$, $0 < x' < b$, which is in the zeroth cell (Figure 2). We use superscript $S$ to denote that the Green's functions include scatterers and obey the boundary conditions on all the scatterers. The single point source Green's function does not obey Bloch condition. The single point source Green's functions can be expressed in terms of the Green's functions of periodic sources $g_{P11}^S(k, k_i, z, z')$ and $g_{P21}^S(k, k_i, z, z')$, where $g_{P11}^S(k, k_i, x, x')$ is the periodic Green's function with field point in region 1 and source point in region 1, while $g_{P21}^S(k, k_i, x, x')$ is the periodic Green's function with field point in region 2 and source point in region 1.

Consider the periodic Green's function equation with source in region 1.

$$\left(\nabla^2 + k_1^2\right) g_{P11}^S(k, k_i, x, x') = -\sum_\alpha \delta(x - x' - \alpha a) e^{ik_i\alpha a} \tag{80}$$

$$\left(\nabla^2 + k^2\right) g_{P21}^S(k, k_i, x, x') = 0 \tag{81}$$

The periodic Green's functions $g_{P11}^S(k, k_i, x, x')$ and $g_{P21}^S(k, k_i, x, x')$ obey Bloch condition and the boundary conditions on all the scatterers.

The First Brillouin Zone (FBZ) is $\frac{-\pi}{a} \leq k_i \leq \frac{\pi}{a}$. Let the eigenfunctions calculated be $\psi_{1\gamma}^S(k_i, x)$ and $\psi_{2\gamma}^S(k_i, x)$ for region 1 and 2, respectively, where $\gamma$ is the band index, and $\gamma = 1, 2, 3, \ldots$. Let the eigenvalues be $k_{0\gamma}(k_i)$. Then

$$g_{P11}^S(k, k_i, x, x') = \sum_\gamma \frac{1}{\left[k_{0\gamma}^{(m)}(k_i)\right]^2 - k_0^2}\psi_{1\gamma}^{S*}(k_i, x')\psi_{1\gamma}^S(k_i, x) \tag{82}$$

$$g_{P21}^S(k, k_i, x, x') = \sum_\gamma \frac{1}{\left[k_{0\gamma}^{(m)}(k_i)\right]^2 - k_0^2}\psi_{1\gamma}^{S*}(k_i, x')\psi_{2\gamma}^S(k_i, x) \tag{83}$$
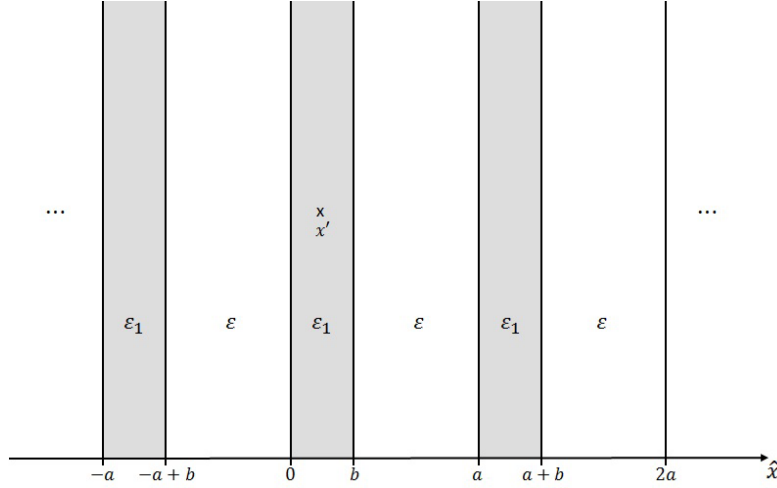
**Figure 2.** The single point source is located at $x'$, $0 < x' < b$, which is in the zeroth cell.

Since we are not calculating the periodic Green's functions, we do not need low wavenumber extractions in the above.

The single point source Green's functions are integrations of the periodic Green's functions over the first Brillouin zone.

$$g_{11}^S \left(k_0, x, x'\right) = \frac{a}{2\pi} \int_{\frac{-\pi}{a}}^{\frac{\pi}{a}} dk_i \sum_\gamma \frac{1}{\left[k_{0\gamma}^{(m)}\left(k_i\right)\right]^2 - k_0^2} \psi_{1\gamma}^{S*}\left(k_i, x'\right) \psi_{1\gamma}^S\left(k_i, x\right) \tag{84}$$

$$g_{21}^S \left(k_0, x, x'\right) = \frac{a}{2\pi} \int_{\frac{-\pi}{a}}^{\frac{\pi}{a}} dk_i \sum_\gamma \frac{1}{\left[k_{0\gamma}^{(m)}\left(k_i\right)\right]^2 - k_0^2} \psi_{1\gamma}^{S*}\left(k_i, x'\right) \psi_{2\gamma}^S\left(k_i, x\right) \tag{85}$$

The Bloch band fields can be expressed in terms of the periodic cell functions $u_{1\gamma}^S\left(k_i, x\right)$ and $u_{2\gamma}^S\left(k_i, x\right)$.

$$\psi_{1\gamma}^S\left(k_i, x\right) = e^{ik_i x} u_{1\gamma}^S\left(k_i, x\right) \tag{86}$$

$$\psi_{2\gamma}^S\left(k_i, x\right) = e^{ik_i x} u_{2\gamma}^S\left(k_i, x\right) \tag{87}$$

Then the single point source Green's function $g_{j1}^S(k_0, x, x')$ can be expressed as, $j = 1, 2$,

$$g_{j1}^S \left(k_0, x, x'\right) = \frac{a}{2\pi} \int_{\frac{-\pi}{a}}^{\frac{\pi}{a}} dk_i \sum_\gamma \frac{e^{ik_i(x-x')}}{\left[k_{0\gamma}^{(m)}\left(k_i\right)\right]^2 - k_0^2} u_{1\gamma}^{S*}\left(k_i, x'\right) u_{j\gamma}^S\left(k_i, x\right); \tag{88}$$

Note that the single point source is located in $0 < x' < b$. However, $x$ can be from negative infinity to positive infinity. To calculate the Green's function $g_{j1}^S(k_0, x, x')$ for $x$ in other cells, we use

$$g_{j1}^S \left(k_0, x + na, x'\right) = \frac{a}{2\pi} \int_{\frac{-\pi}{a}}^{\frac{\pi}{a}} dk_i \sum_\gamma \frac{e^{ik_i(x+na-x')}}{\left[k_{0\gamma}^{(m)}\left(k_i\right)\right]^2 - k_0^2} u_{1\gamma}^{S*}\left(k_i, x'\right) u_{j\gamma}^S\left(k_i, x\right) \tag{89}$$

where $x$ is in the zeroth cell with $0 < x < a$.

### 3.1. Extended Zone Representation

A band diagram is shown in Figure 3. The eigenvalues $k_0$ are plotting as a function of $k_i$ in the first Brillouin zone. In the FBZ, all the bands are found. An alternative is to use the extended zone representation [25] with $-\infty < k_i < \infty$ where the higher bands are translated to their respective
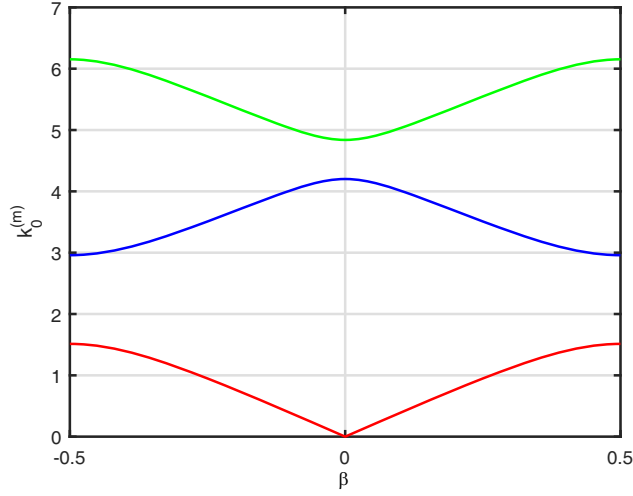
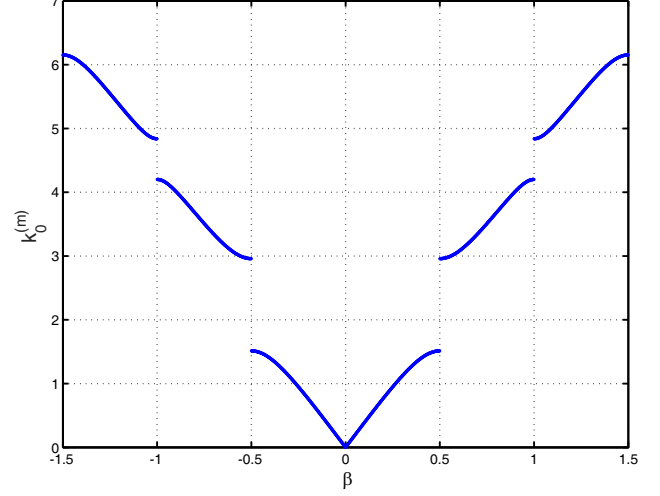**Figure 3.** Band diagram in the first Brioullin zone (FBZ).



**Figure 4.** Band diagram in the extended zone representation.

zone. An extended zone representation of band diagram is shown in Figure 4. In the extended zone representation, there is only one band for each $k_i$. Then there is no $\gamma$ index. In the extended zone, then

$$g_{j1}^{S}\left(k_0, x, x'\right) = \frac{a}{2\pi} \int_{-\infty}^{\infty} dk_i \frac{e^{ik_i(x-x')}}{\left[k_0^{(m)}\left(k_i\right)\right]^2 - k_0^2} u_1^{S*}\left(k_i, x'\right) u_j^{S}\left(k_i, x\right) \tag{90}$$

We add superscript "$m$" to denote "mode" eigenvalue. Using this representation, the point source Green's function resembles that of free space Green's function except the unity terms are replaced by cell functions $u_1^{S}(k_i, x)$ and $u_2^{S}(k_i, x)$. An advantage of using extended zone representation is that when $k_0$ is in the passband, then there is a pole due to the term $\frac{1}{[k_0^{(m)}(k_i)]^2 - k_0^2}$ corresponding to the passband mode and, by performing contour integration, the residue of the mode can be calculated.

### 3.2. Low Wavenumber Mid-Bandgap Extraction

The convergence of the expansion $\sum_\gamma \frac{1}{k_{0\gamma}^2(k_i) - k_0^2}$ is slow and decreases as $\sum_\gamma \frac{1}{k_{0\gamma}^2(k_i)}$. This is due to near field effects and evanescent waves. In the past we use a low wavenumber extraction with $k_0 = k_L$ close to zero. However, for this case of periodic structure, the $k_0$ close to zero can be in the passband. For passband, the fields are extended to infinity. On the other hand, for $k_0$ in the bandgap, the fields are confined to a few cells. Thus for convenience, we choose the low wavenumber to be in the lowest mid-bandgap so that the mode field decays with distance. Let $k_L = k_g$, where the single $k_g$ is in the bandgap, and roughly in the mid bandgap. Thus the $k_L$ may not be low compared with operating wavenumber $k_0$. It is actually higher than passband. Nevertheless, $k_L$ is low compared with the highest mode wavenumber when the summation or integration is truncated. Then we have

$$g_{j1}^{S}\left(k_0, x, x'\right) = g_{j1}^{S}\left(k_g, x, x'\right) + \frac{a}{2\pi} \int_{\frac{-\pi}{a}}^{\frac{\pi}{a}} dk_i e^{ik_i(x-x')}$$

$$\times \sum_\gamma \left\{ \frac{1}{\left[k_{0\gamma}^{(m)}\left(k_i\right)\right]^2 - k_0^2} - \frac{1}{\left[k_{0\gamma}^{(m)}\left(k_i\right)\right]^2 - k_g^2} \right\} u_{1\gamma}^{S*}\left(k_i, x'\right) u_{j\gamma}^{S}\left(k_i, x\right) \tag{91}$$

The above summation has accelerated convergence and decreases as $\sum_\gamma \frac{1}{k_{0\gamma}^4(k_i)}$. Another advantage is that the bandgap point source wave function at $k_g$ is relatively easy to compute as it requires few number of layers to compute the Green's function.

Our computational procedures of point source Green's functions proceed as follows.

### 3.3. Case of $k_0$ in Bandgap

Since both $k_0$ and $k_g$ are in the bandgap, we compute using the original expressions given above.

### 3.4. Case of $k_0$ in Bandpass

For simplicity, we are studying the lowest passband $\gamma = 1$. Then there is a pole on the path of integration. The pole is

$$k_{0\gamma}^{(m)}(k_{i0}) = k_0 \tag{92}$$

We introduce an artificial small loss of $\epsilon$ in $k_0$. As stated in the Introduction, by lossless case, we first define a maximum distance of interest. Then, 1) within the maximum distance of interest, the Green's function behaves as in the lossless (infinitesimal loss) case, and 2) within the maximum distance, the Green's function is independent of the artificial loss $\epsilon$ put in the simulations. We use two procedures and the computed results are compared with each other to ensure accuracy.

**Procedure 1: Introducing A Small Loss $\epsilon$**

Equation (91) becomes with an artificial small loss $\epsilon$. Then integration is carried out in the FBZ. Because of the pole singularity, the integrands are sharply peaked at $k_i = k_{i0}$.

$$g_{j1}^S(k_0, x, x') = g_{j1}^S(k_g, x, x') + \frac{a}{2\pi} \int_{-\frac{\pi}{a}}^{\frac{\pi}{a}} dk_i e^{ik_i(x-x')}$$

$$\times \sum_\gamma \left\{ \frac{1}{k_{0\gamma}^2(k_i) - [k_0(1+i\epsilon)]^2} - \frac{1}{k_{0\gamma}^2(k_i) - k_g^2} \right\} u_{1\gamma}^{S*}(k_i, x') u_{j\gamma}^S(k_i, x) \tag{93}$$

We assume that, in real practice, the maximum separation $|x - x'|$ is at most 50 cells. The choice of $\epsilon$ is small enough that the solution is close to the lossless case for maximum distance of 50 cells. The integral is calculated numerically.

**Procedure 2: Modal Approach with First Order Pole Extractions for Passband**

Without loss of generality, let $k_0$ be in the first passband. Then we have, using extended zone,

$$g_{j1}^S(k_0, x, x') = g_{j1}^S(k_g, x, x') + \frac{a}{2\pi} \int_{-\infty}^{\infty} dk_i e^{ik_i(x-x')}$$

$$\times \left\{ \frac{1}{\left[k_0^{(m)}(k_i)\right]^2 - [k_0(1+i\epsilon)]^2} - \frac{1}{k_0^2(k_i) - k_g^2} \right\} u_1^{S*}(k_i, x') u_j^S(k_i, x) \tag{94}$$

There are 2 poles that are near $k_i = \pm k_{i0}$. The actual poles are in the complex $k_i$-plane. The values of $k_{i0}$ are such that

$$k_0^{(m)}(\pm k_{i0}) = k_0 \tag{95}$$

Let the first derivative of $k_0^{(m)}(k_i)$ at $k_{i0}$ be

$$\left[ \frac{d}{dk_i} k_0^{(m)}(k_i) \right]_{k_i = k_{i0}} = k_0^{(m)\prime}(k_{i0}) \tag{96}$$

Because of symmetry for positive and negative $k_i$, we have

$$k_0^{(m)\prime}(-k_{i0}) = -k_0^{(m)\prime}(k_{i0}) \tag{97}$$

The residue at $k_i = k_{i0}$ is given by

$$\text{Resid}_j(k_{i0}, x, x') = \frac{u_1^{S*}(k_{i0}, x') u_j^S(k_{i0}, x)}{2k_0 k_0^{(m)\prime}(k_{i0})} \tag{98}$$

and the residue at $k_i = -k_{i0}$ is

$$\text{Resid}\left(-k_{i0}, x, x'\right) = -\left[\text{Resid}\left(k_{i0}, x, x'\right)\right]^* \tag{99}$$

**1) Positive $k_i$ axis:** In the vicinity of $k_{i0}$,

$$k_0^{(m)}\left(k_i\right) = k_0 + k_0^{(m)\prime}\left(k_{i0}\right)\left(k_i - k_{i0}\right) \tag{100}$$

Then we can write

$$\frac{u_1^{S*}\left(k_i, x'\right) u_j^S\left(k_i, x\right)}{\left[k_0^{(m)}\left(k_i\right)\right]^2 - \left[k_0\left(1 + i\epsilon\right)\right]^2} \simeq \frac{u_1^{S*}\left(k_{i0}, x'\right) u_j^S\left(k_{i0}, x\right)}{\left[k_0^{(m)\prime}\left(k_{i0}\right)\left(k_i - k_{i0}\right) - i\epsilon k_0\right] 2k_0}$$

$$= \frac{\text{Resid}_j\left(k_{i0}, x, x'\right)}{\left(k_i - k_{i0}\right) - \dfrac{i\epsilon k_0}{k_0^{(m)\prime}\left(k_{i0}\right)}} \tag{101}$$

The pole is in the complex plane off the real $k_i$ axis.

$$k_i = k_{i0} + \frac{i\epsilon k_0}{k_0^{(m)\prime}\left(k_{i0}\right)} \tag{102}$$

**2) Negative $k_i$ axis:** In the vicinity of $-k_{i0}$,

$$k_0^{(m)}\left(k_i\right) = k_0 + k_0^{(m)\prime}\left(-k_{i0}\right)\left(k_i + k_{i0}\right) = k_0 - k_0^{(m)\prime}\left(k_{i0}\right)\left(k_i + k_{i0}\right) \tag{103}$$

Then we have

$$\frac{u_1^{S*}\left(k_i, x'\right) u_j^S\left(k_i, x\right)}{\left[k_0^{(m)}\left(k_i\right)\right]^2 - \left[k_0\left(1 + i\epsilon\right)\right]^2} \simeq \frac{\text{Resid}\left(-k_{i0}, x, x'\right)}{k_i + k_{i0} + \dfrac{i\epsilon k_0}{k_0^{(m)\prime}\left(k_{i0}\right)}} \tag{104}$$

Using the residues in Eqs. (98) and (99), Eq. (94) can be rewritten as

$$g_{j1}^S\left(k_0, x, x'\right) = g_{j1}^S\left(k_g, x, x'\right) + \frac{a}{2\pi} \int_{-\infty}^{\infty} dk_i e^{ik_i(x-x')} \left\{ \frac{u_1^{S*}\left(k_i, x'\right) u_j^S\left(k_i, x\right)}{\left[k_0^{(m)}\left(k_i\right)\right]^2 - \left[k_0\left(1 + i\epsilon\right)\right]^2} \right.$$

$$\left. - \frac{u_1^{S*}\left(k_i, x'\right) u_j^S\left(k_i, x\right)}{k_0^2\left(k_i\right) - k_g^2} - \frac{\text{Resid}_j\left(k_{i0}, x, x'\right)}{k_i - k_{i0} - \dfrac{i\epsilon k_0}{k_0^{(m)\prime}\left(k_{i0}\right)}} - \frac{\text{Resid}\left(-k_{i0}, x, x'\right)}{k_i + k_{i0} + \dfrac{i\epsilon k_0}{k_0^{(m)\prime}\left(k_{i0}\right)}} \right\} + I_m \tag{105}$$

where $I_m$ is the modal solution.

$$I_m = \frac{a}{2\pi} \int_{-\infty}^{\infty} dk_i e^{ik_i(x-x')} \left[ \frac{\text{Resid}_j\left(k_{i0}, x, x'\right)}{\left(k_i - k_{i0}\right) - \dfrac{i\epsilon k_0}{k_0^{(m)\prime}\left(k_{i0}\right)}} + \frac{\text{Resid}\left(-k_{i0}, x, x'\right)}{k_i + k_{i0} + \dfrac{i\epsilon k_0}{k_0^{(m)\prime}\left(k_{i0}\right)}} \right] \tag{106}$$

We further write the second term in Eq. (105) as the sum of two integrals $I_1$ and $I_2$.

$$g_{j1}^S\left(k_0, x, x'\right) = g_{j1}^S\left(k_g, x, x'\right) + I_1 + I_2 + I_m \tag{107}$$

with

$$I_1 = \frac{a}{2\pi} \int_{-\frac{\pi}{a}}^{\frac{\pi}{a}} dk_i e^{ik_i(x-x')} \left\{ \sum_\gamma \left[ \frac{1}{k_{0\gamma}^2\left(k_i\right) - \left[k_0\left(1 + i\epsilon\right)\right]^2} - \frac{1}{k_{0\gamma}^2\left(k_i\right) - k_g^2} \right] u_{1\gamma}^{S*}\left(k_i, x'\right) u_{j\beta}^S\left(k_i, x\right) \right.$$

$$\left. - \left[ \frac{\text{Resid}_j\left(k_{i0}, x, x'\right)}{k_i - k_{i0} - \dfrac{i\epsilon k_0}{k_0^{(m)\prime}\left(k_{i0}\right)}} + \frac{\text{Resid}\left(-k_{i0}, x, x'\right)}{k_i + k_{i0} + \dfrac{i\epsilon k_0}{k_0^{(m)\prime}\left(k_{i0}\right)}} \right] \right\} \tag{108}$$

and

$$I_2 = -\frac{a}{2\pi} \left( \int_{-\infty}^{-\frac{\pi}{a}} + \int_{\frac{\pi}{a}}^{\infty} \right) dk_i e^{ik_i(x-x')} \left[ \frac{\mathrm{Resid}_j\left(k_{i0}, x, x'\right)}{k_i - k_{i0} - \dfrac{i\epsilon k_0}{k_0^{(m)\prime}\left(k_{i0}\right)}} + \frac{\mathrm{Resid}\left(-k_{i0}, x, x'\right)}{k_i + k_{i0} + \dfrac{i\epsilon k_0}{k_0^{(m)\prime}\left(k_{i0}\right)}} \right] \qquad (109)$$

Note that the above is exact as we only subtract and add terms. The integral $I_1$ is over the FBZ and is computed numerically as before. The integrand is much smoother because the two poles near $+k_{i0}$ and $-k_{i0}$ have been extracted. The integral $I_2$ can be expressed as exponential integral. Let

$$J(q, y, b) = \int_q^{\infty} dk_i \frac{e^{ik_i y}}{k_i + b} = e^{iqy} e^{-iy(q+b)} E_1\left(-iy\left(q+b\right)\right) \qquad (110)$$

where $E_1(x)$ is the exponential integral function defined as

$$E_1(x) = \int_x^{\infty} dt \frac{e^{-t}}{t} \qquad (111)$$

Then $I_2$ becomes

$$I_2 = -\frac{a}{2\pi} \left\{ J\left(\frac{\pi}{a}, x - x', -k_{i0} - \frac{i\epsilon k_0}{k_0^{(m)\prime}\left(k_{i0}\right)}\right) \mathrm{Resid}_j\left(k_{i0}, x, x'\right) \right.$$
$$+ J\left(\frac{\pi}{a}, x' - x, -k_{i0} - \frac{i\epsilon k_0}{k_0^{(m)\prime}\left(k_{i0}\right)}\right) \left[\mathrm{Resid}\left(k_{i0}, x, x'\right)\right]^* \right\}$$
$$+ \frac{a}{2\pi} \left\{ J\left(\frac{\pi}{a}, x - x', k_{i0} + \frac{i\epsilon k_0}{k_0^{(m)\prime}\left(k_{i0}\right)}\right) \left[\mathrm{Resid}\left(k_{i0}, x, x'\right)\right]^* \right.$$
$$\left. + J\left(\frac{\pi}{a}, x' - x, k_{i0} + \frac{i\epsilon k_0}{k_0^{(m)\prime}\left(k_{i0}\right)}\right) \mathrm{Resid}_j\left(k_{i0}, x, x'\right) \right\} \qquad (112)$$

The modal solution $I_m$ can be calculated by residue calculus. For $x > x'$, we deform the contour upward and capture the pole at $[k_{i0} + \frac{k_0 i\epsilon}{k_0^{(m)\prime}(k_{i0})}]$. For $x < x'$, we deform downward and capture the pole at $-[k_{i0} + \frac{k_0 i\epsilon}{k_0^{(m)\prime}(k_{i0})}]$.

$$I_m = \begin{cases} ia\mathrm{Resid}_j\left(k_{i0}, x, x'\right) e^{i\left[k_{i0} + \frac{i\epsilon k_0}{k_0^{(m)\prime}(k_{i0})}\right](x-x')} & \text{for } x > x' \\[3mm] -ia\mathrm{Resid}\left(-k_{i0}, x, x'\right) e^{-i\left[k_{i0} + \frac{i\epsilon k_0}{k_0^{(m)\prime}(k_{i0})}\right](x-x')} & \text{for } x < x' \end{cases} \qquad (113)$$

## 3.5. Modal Approach with Second Order Pole Extractions Near Band Edge

Near the bandedge the group velocity represented by the first derivative of the band diagram $k_0^{(m)\prime}(k_i)$ is small. The group velocity is actually zero at the band edge of $\beta = \pm 0.5$. Thus near the bandedge, we use both first order derivative $k_0^{(m)\prime}(k_i)$ and second order derivative $k_0^{(m)\prime\prime}(k_i)$.

Near the positive edge $\beta = 0.5$, the approximation of the singularity near $k_{i0}$ is

$$\frac{1}{\left[k_0^{(m)}\left(k_i\right)\right]^2 - \left[k_0\left(1 + i\epsilon\right)\right]^2} \simeq \frac{1}{2k_0 k_m'\left(k_{i0}\right)\left[\left(k_i - k_{i0}\right) - \dfrac{i\epsilon k_0}{k_m'\left(k_{i0}\right)} + \dfrac{1}{2}\dfrac{k_m''\left(k_{i0}\right)}{k_m'\left(k_{i0}\right)}\left(k_i - k_{i0}\right)^2\right]} \qquad (114)$$

Since $k_0^{(m)}(k_i)$ is an even function, the approximation of the singularity near $-k_{i0}$ is

$$\frac{1}{\left[k_0^{(m)}\left(k_i\right)\right]^2 - \left[k_0\left(1 + i\epsilon\right)\right]^2} \simeq \frac{1}{-2k_0 k_m'\left(k_{i0}\right)\left[k_i + k_{i0} + \dfrac{i\epsilon k_0}{k_m'\left(k_{i0}\right)} - \dfrac{1}{2}\dfrac{k_m''\left(k_{i0}\right)}{k_m'\left(k_{i0}\right)}\left(k_i + k_{i0}\right)^2\right]} \qquad (115)$$

We notice that the quadratic terms in the denominator mean that there are two poles, $k_{P1}$ and $k_{P2}$.

$$k_{P1} = k_{i0} - \frac{k'_m (k_{i0})}{k''_m (k_{i0})} + \sqrt{\left[\frac{k'_m (k_{i0})}{k''_m (k_{i0})}\right]^2 + \frac{2i\epsilon k_0}{k''_m (k_{i0})}} \tag{116}$$

$$k_{P2} = k_{i0} - \frac{k'_m (k_{i0})}{k''_m (k_{i0})} - \sqrt{\left[\frac{k'_m (k_{i0})}{k''_m (k_{i0})}\right]^2 + \frac{2i\epsilon k_0}{k''_m (k_{i0})}} \tag{117}$$

The pole $k_{P1}$, has $\mathrm{Im}\,(k_{P1}) > 0$ and $0 < \mathrm{Re}\,(k_{P1}) < \frac{\pi}{a}$. The pole $k_{P2}$, has $\mathrm{Im}\,(k_{P2}) < 0$ and $\frac{\pi}{a} < \mathrm{Re}\,(k_{P2}) < \frac{2\pi}{a}$.

We perform the integrations with the following formulas. The extraction, as in Eq. (107), is exact as we merely subtract and add the same terms. With the second order pole extractions, the integrals $I_1$ and $I_2 + I_m$ become, respectively,

$$I_1 = \frac{a}{2\pi} \int_{-\frac{\pi}{a}}^{\frac{\pi}{a}} dk_i e^{ik_i(x-x')} \left\{ \sum_\gamma \left[ \frac{1}{\left[k_{0\gamma}^{(m)} (k_i)\right]^2 - [k_0 (1 + i\epsilon)]^2} - \frac{1}{\left[k_{0\gamma}^{(m)} (k_i)\right]^2 - k_g^2} \right] u_{1\beta}^{S*} (k_i, x')\, u_{j\beta}^{S} (k_i, x) \right\}$$
$$- \frac{a}{2\pi} \frac{2k'_m (k_{i0})}{k''_m (k_{i0})} \int_{-\frac{\pi}{a}}^{\frac{\pi}{a}} dk_i e^{ik_i(x-x')} \left\{ \frac{\mathrm{Resid}_j (k_{i0}, x, x')}{(k_i - k_{P1})(k_i - k_{P2})} + \frac{[\mathrm{Resid}_j (k_{i0}, x, x')]^*}{(k_i + k_{P1})(k_i + k_{P2})} \right\} \tag{118}$$

and

$$I_2 + I_m = \frac{a}{2\pi} \frac{2k'_m (k_{i0})}{k''_m (k_{i0})} \int_{-\frac{\pi}{a}}^{\frac{\pi}{a}} dk_i e^{ik_i(x-x')} \left\{ \frac{\mathrm{Resid}_j (k_{i0}, x, x')}{(k_i - k_{P1})(k_i - k_{P2})} + \frac{[\mathrm{Resid}_j (k_{i0}, x, x')]^*}{(k_i + k_{P1})(k_i + k_{P2})} \right\} \tag{119}$$

Using

$$\frac{1}{(k_i - k_{P1})(k_i - k_{P2})} = \frac{1}{k_{P1} - k_{P2}} \left[ \frac{1}{k_i - k_{P1}} - \frac{1}{k_i - k_{P2}} \right] \tag{120}$$

$$\frac{1}{(k_i + k_{P1})(k_i + k_{P2})} = \frac{1}{k_{P2} - k_{P1}} \left[ \frac{1}{k_i + k_{P1}} - \frac{1}{k_i + k_{P2}} \right] \tag{121}$$

the decomposition of the right hand side of Eq. (119) is such that the integral $I_m$ is chosen to account for the modes at $\pm k_{P1}$ with $\int_{-\infty}^{\infty} dk_i e^{ik_i(x-x')}$.

$$I_m = \frac{a}{2\pi} \frac{2k'_m (k_{i0})}{k''_m (k_{i0})} \frac{1}{k_{P1} - k_{P2}} \int_{-\infty}^{\infty} dk_i e^{ik_i(x-x')} \left\{ \frac{\mathrm{Resid}_j (k_{i0}, x, x')}{k_i - k_{P1}} - \frac{[\mathrm{Resid}_j (k_{i0}, x, x')]^*}{k_i + k_{P1}} \right\} \tag{122}$$

The remainder of the right side of Eq. (119) goes to $I_2$ with

$$I_2 = I_{21} + I_{22} \tag{123}$$

where

$$I_{21} = \frac{a}{\pi} \frac{k'_m (k_{i0})}{k''_m (k_{i0})} \frac{1}{k_{P1} - k_{P2}} \int_{\frac{\pi}{a}}^{\infty} dk_i \left\{ e^{-ik_i(x-x')} \frac{\mathrm{Resid}_j (k_{i0}, x, x')}{k_i + k_{P1}} - e^{ik_i(x-x')} \frac{\mathrm{Resid}_j (k_{i0}, x, x')}{k_i - k_{P1}} \right.$$
$$\left. - e^{-ik_i(x-x')} \frac{[\mathrm{Resid}_j (k_{i0}, x, x')]^*}{k_i - k_{P1}} + e^{ik_i(x-x')} \frac{[\mathrm{Resid}_j (k_{i0}, x, x')]^*}{k_i + k_{P1}} \right\} \tag{124}$$

and

$$I_{22} = \frac{a}{\pi} \frac{k'_m (k_{i0})}{k''_m (k_{i0})} \frac{1}{k_{P1} - k_{P2}} \int_{-\frac{\pi}{a}}^{\frac{\pi}{a}} dk_i e^{ik_i(x-x')} \left\{ -\frac{\mathrm{Resid}_j (k_{i0}, x, x')}{k_i - k_{P2}} + \frac{[\mathrm{Resid}_j (k_{i0}, x, x')]^*}{k_i + k_{P2}} \right\} \tag{125}$$

For $k_{P2}$, the pole is to the right of $\frac{\pi}{a}$, thus we avoid that region. For $-k_{P2}$, the pole is to the left of $\frac{-\pi}{a}$, thus we avoid that region. Using the definition of $J$ integral of Eq. (110), it follows that

$$I_{21} = \frac{a}{2\pi} \frac{2k'_m(k_{i0})}{k''_m(k_{i0})} \frac{1}{k_{P1} - k_{P2}} \left\{ \text{Resid}_j(k_{i0}, x, x') J\left(\frac{\pi}{a}, x' - x, k_{P1}\right) \right.$$
$$- \text{Resid}_j(k_{i0}, x, x') J\left(\frac{\pi}{a}, x - x', -k_{P1}\right)$$
$$\left. - \left[\text{Resid}_j(k_{i0}, x, x')\right]^* J\left(\frac{\pi}{a}, x' - x, -k_{P1}\right) + \left[\text{Resid}_j(k_{i0}, x, x')\right]^* J\left(\frac{\pi}{a}, x - x', k_{P1}\right) \right\} \quad (126)$$

and

$$I_{22} = \frac{a}{2\pi} \frac{2k'_m(k_{i0})}{k''_m(k_{i0})} \frac{1}{k_{P1} - k_{P2}} \left\{ \text{Resid}_j(k_{i0}, x, x') J\left(\frac{-\pi}{a}, x' - x, k_{P2}\right) \right.$$
$$- \text{Resid}_j(k_{i0}, x, x') J\left(\frac{\pi}{a}, x' - x, k_{P2}\right)$$
$$\left. + \left[\text{Resid}_j(k_{i0}, x, x')\right]^* J\left(\frac{-\pi}{a}, x - x', k_{P2}\right) - \left[\text{Resid}_j(k_{i0}, x, x')\right]^* J\left(\frac{\pi}{a}, x - x', k_{P2}\right) \right\} \quad (127)$$

The modal solution $I_m$ can be obtained by taking residues.

$$I_m = \begin{cases} \dfrac{i2ak'_m(k_{i0})}{k''_m(k_{i0})(k_{P1} - k_{P2})} e^{ik_{P1}(x-x')} \text{Resid}_j(k_{i0}, x, x') & \text{for } x > x' \\[4mm] \dfrac{i2ak'_m(k_{i0})}{k''_m(k_{i0})(k_{P1} - k_{P2})} e^{-ik_{P1}(x-x')} \left[\text{Resid}_j(k_{i0}, x, x')\right]^* & \text{for } x < x' \end{cases} \quad (128)$$

## 4. NUMERICAL RESULTS

We illustrate numerical results in this section. The parameters are chosen as follows: $b = 0.2a$, $\varepsilon_1 = 8.9\varepsilon_0$ and $\varepsilon = \varepsilon_0$. For the case of the single point source, the location of source is at $x' = 0.1a$. Let the normalized Bloch wave vector be $\beta = k_i \frac{a}{2\pi}$. Thus, the first Brillouin zone is $\frac{-1}{2} \leq \beta \leq \frac{1}{2}$. In the following, we set the lattice constant $a = 1$ so that everything is unit-less and ready to scale.

### 4.1. Band Diagrams

In applying BBGFL to calculate band eigenvalues and band field solutions, we used $k_{0L} = 0.001(\frac{2\pi}{a})$. In Figure 3, we plot the band structure in the FBZ for band eigenvalue $k_0^{(m)}$ as a function of $\beta$, with $m$ being the band index. The key numbers for subsequent results are 1) the lowest band is the passband with the lowest point at $\beta = 0$, 2) The bandedge is at $\beta = \pm 0.5$ with band eigenvalue $k_0^{(m)} = 1.51273$. In the illustration of numerical results, we choose mid-bandgap as $k_L = k_g = 2.3$. In Figure 4, we show the band diagram of Figure 2, using the extended zone representation [25].

### 4.2. Comparison of Band Field Solution between BBGFL and Plane Wave Method

A common method of calculating band solution is the plane wave method [22, 24]. It is noted in BBGFL that the band mode solution is a sum of the boundary term (low wavenumber contribution) and the plane wave expansion (fast-converging modal summation). On the other hand, the plane wave method only contains the plane wave expansion. It is known that the plane wave method gives Gibbs oscillation because of boundary discontinuities. Various methods have been proposed to smooth out the discontinuities [24] in the plane wave method. Most of the works focused on the eigenvalues. However, the point Green's functions are expressed in terms of band field solutions. Thus accurate band field solutions are required. In the following, we compare the BBGFL band field solutions with the plane wave method and the ABCD method [21]. In the ABCD method, the band eigenvalue and band field solutions are determined by a nonlinear eigenvalue problem.
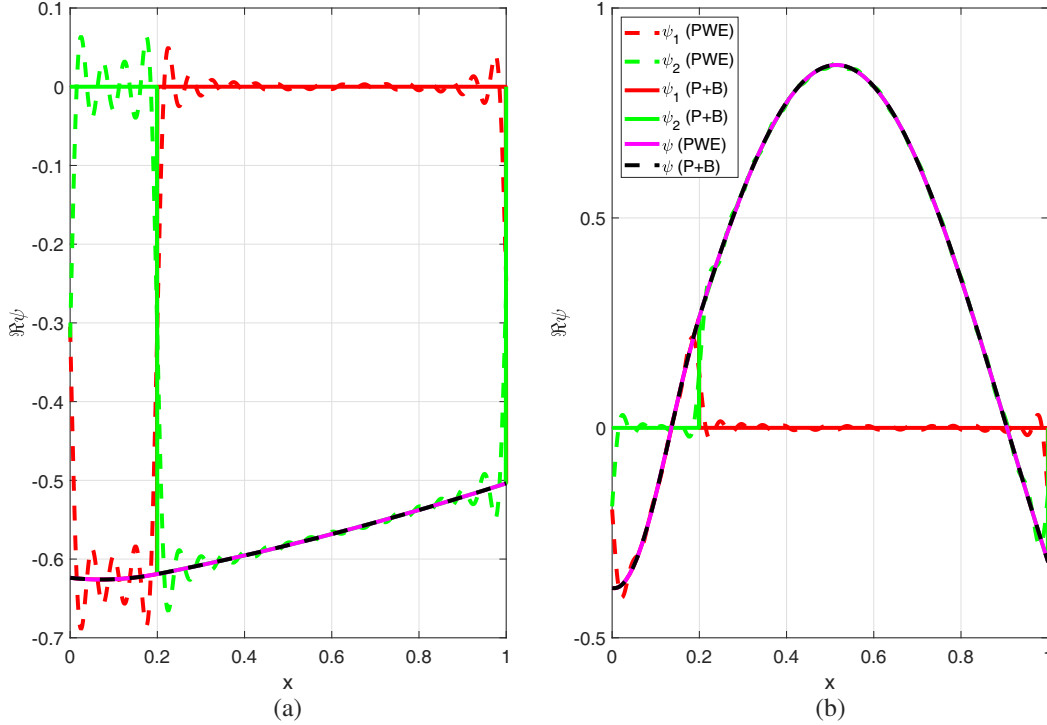
**Figure 5.** Band solution from BBGFL: Contributions from the plane-wave expansions (PWE) compared with the sum of the plane-wave expansions and the boundary term (P + B). (a) The first mode at $k_\gamma = 0.0621\frac{2\pi}{a}$, (b) the second mode at $k_\gamma = 0.6386\frac{2\pi}{a}$. The Bloch wave vector is chosen at $k_i = 0.1001\frac{2\pi}{a}$. The Floquet plane-wave series in BBGFL are truncated at $N = 20$.

In Figure 5, we evaluate the contribution to the band field solution from the boundary term in the BBGFL formulation. It is clear that without the boundary term, the truncated plane wave expansion in Eq. (53) calculates $\psi_1$ and $\psi_2$ that suffer Gibbs oscillations and the fields extend out its validity domain. With the boundary term in Eqs. (48) and (49), however, the Gibbs oscillations in $\psi_1$ and $\psi_2$ disappear and both fields vanish outside its validity domain. The fact that physical modes have $\psi_1$ vanishing in region 2, and $\psi_2$ vanishing in region 1 can be used to reject potential non-physical spurious modes. Interestingly, the Gibbs oscillations in $\psi_1$ and $\psi_2$ from the truncated plane wave expansion in Eq. (53) cancel each other so that when they are added up to produce $\psi = \psi_1 + \psi_2$, the results are almost identical to the results when the boundary term contributions are included with Eqs. (48) and (49). In using BBGFL to determine band eigenvalue and band field solution, we choose the low wavenumber $k_{0L} = 0.0062832$.

In Figure 6, we compare the band field solution computed from the BBGFL method and the plane wave expansion (PWE) method [22]. The results of the ABCD method [21] are also included as benchmark solutions. In the BBGFL method, we truncate the Floquet plane wave series at $N = 20$, while in the plane wave expansion method, we truncate the series at $N = 20$, 100, and 250, respectively. It is noted that the BBGFL solutions are in excellent agreement with that of the ABCD method, and the fields have smooth transitions at the medium boundaries. On the other hand, the plane wave method produces Gibbs phenomena, and it requires much larger number of Floquet plane waves to converge. Thus, the BBGFL method is associated with a much smaller linear eigenvalue problem than the plane wave expansion method, and it also produces much more accurate band mode solutions than the plane wave expansion method.
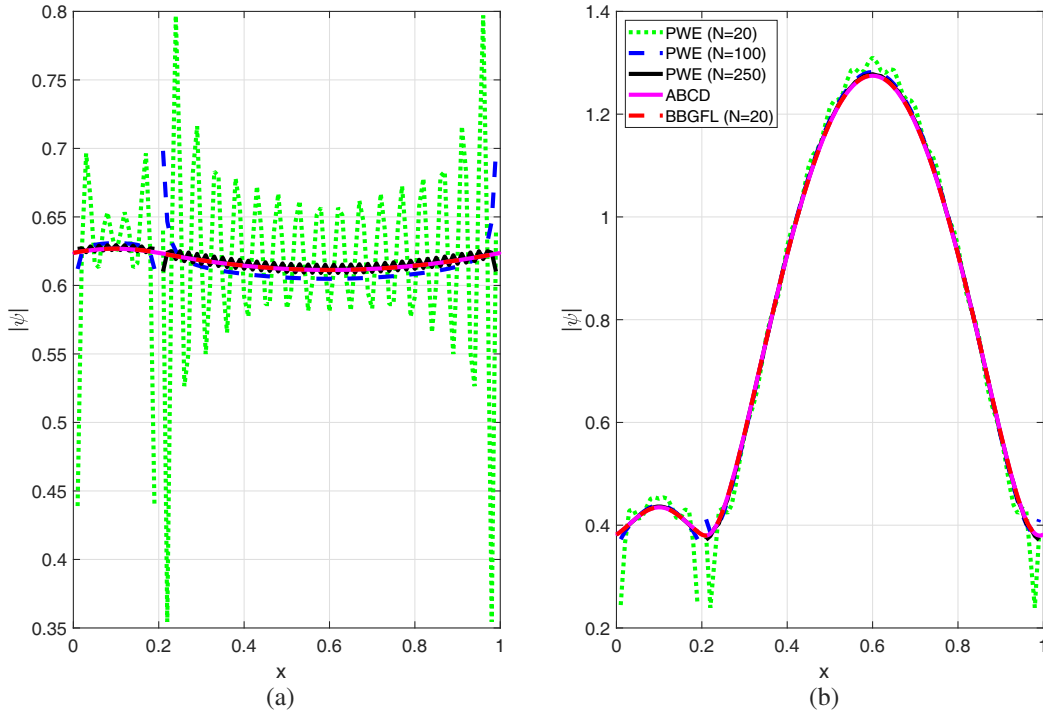
**Figure 6.** Band solution from BBGFL compared with plane-wave expansion (PWE) method and the ABCD method: (a) the first mode at $k_\gamma = 0.0621\frac{2\pi}{a}$, (b) the second mode at $k_\gamma = 0.6386\frac{2\pi}{a}$. The Bloch wave vector is chosen at $k_i = 0.1001\frac{2\pi}{a}$. The Floquet plane-wave series in BBGFL are truncated at $N = 20$. The plane-wave series in PWE are truncated at $N = 20, 100$, and 250, respectively.

## 4.3. Point Source Green's Function Bench Mark Solution Based on Scattering Method

The usual scattering method consists of solving the wave equation and boundary conditions for each wavenumber, one at a time. The physics of the solution is the inclusion of all the multiple scattering solution of all the scatterers. There are extensive multiple scattering in a periodic structure. On the other hand, the Broadband Green's function are expressed in band solution with each band solution already containing all the multiple scattering. The scattering solution serves as a bench mark comparison with the Broadband Green's function method.

In computing the scattering solution, the point source is placed at $x' = 0.1$. We used a total of 200,000 layers with 100,000 layers on each side of the point source. The maximum distance of interest for the Green's function is 50 cells. An artificial loss is put in $\varepsilon_1$, $\varepsilon_1 = 8.9\varepsilon_0(1 + i\epsilon_{bm})$, where "$bm$" stands for the benchmark. Two cases are computed with $\beta = 0.1$ and 0.49.

1) $k_0 = 0.38958$. This is in the passband with $k_{i0} = 0.62831$ and $\beta_0 = k_{i0}\frac{a}{2\pi} = 0.1$. For the mode method, we also need to compute the slope which is $k_0^{(m)\prime}(0.62831) = 0.614833$.

2) $k_0 = 1.511473682$. This is in the passband very close to the bandedge with $k_{i0} = 3.0787608$ and $\beta_0 = 0.49$. The computed slope is $k_0^{(m)\prime}(3.110177) = 0.039935$. The slope is quite small near the bandedge.

The case of $\beta_0 = 0.49$ is very close to the bandedge $\beta = 0.5$. For the case of $\beta_0 = 0.1$, an artificial loss of $\epsilon_{bm} = 0.001$ is sufficient. However, the case of $\beta_0 = 0.49$ requires much smaller loss. In Figures 7(a) and 7(b), we show the benchmark scattering solution for this case with $\epsilon_{bm}$. The Figures 7(a) and 7(b) are respectively for $0 \le x \le 1$ and $0 \le x \le 50$. The figure shows that the results for lossless case are with $\epsilon_{bm} = 0.00005$ and $\epsilon_{bm} = 0.00002$, while $\epsilon_{bm} = 0.001$ gives incorrect results because of coupling to the bandgap when the wavenumber is very close to the band edge.
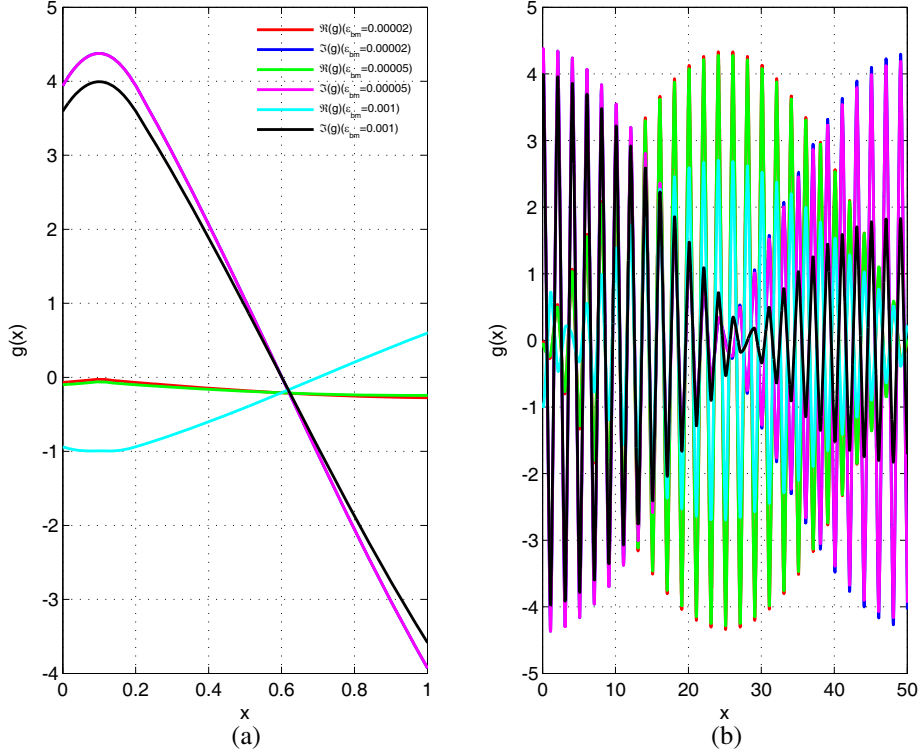
**Figure 7.** Bench mark Green's functions for lossless case and $\beta_0 = 0.49$ are with an artifical loss $\epsilon_{bm} = 0.001$, $\epsilon_{bm} = 0.00005$, and $\epsilon_{bm} = 0.00002$. (a) $0 \le x \le 1$ and (b) $0 \le x \le 50$.

### 4.4. Mid-Bandgap Solution in One-Time Setup $g_{j1}^S (k_g, x, x')$

The BBGFL solution requires a one-time setup of calculating the band solutions as described above and the low wavenumber mid-bandgap solution, $g_{j1}^S(k_g, x, x')$. The source is in medium 1 at $x' = 0.1$, while the field point $x$ is in $j = 1, 2$ corresponding to the respective medium 1 and 2. The midband point source Green's function is computed quite readily from the benchmark scattering solution using the scattering method. This is because the solution has a finite extent, since $k_L = k_g = 2.3$ is in mid-bandgap. Figure 8 shows the point source Green's functions for $0 \le x \le 5$, with $x' = 0.1$. The results shows that the Green's function is limited in spatial extent. In computing the scattering solution, we only need to use 30 layers on each side.

With the setup completed, we can compute the broadband point source Green's function for any wavenumber $k_0$ by merely varying the $k_0$ in the denominator of Eq. (44). We illustrate 3 cases: 1) stopband with $k_0 = 2.0$, 2) passband with $k_0 = 0.38958$ ($\beta = 0.1$), and 3) very close to the bandedge with $k_0 = 1.511473$ ($\beta = 0.49$).

#### 4.4.1. Stopband $k_0 = 2$

The solution is computed by equation with the mid-bandgap extraction. The computation is performed over the first Brillouin zone. In Figure 9, we plot the point source Green's function and compare with the scattering benchmark solution. The two results are indistinguishable.

#### 4.4.2. Passband $k_0 = 0.38958$

We use the modal approach with first order pole extraction. The integral $I_1$ is performed numerically over the FBZ. We choose the artificial loss to be $\epsilon = 10^{-5}$. The integrand has the term without the
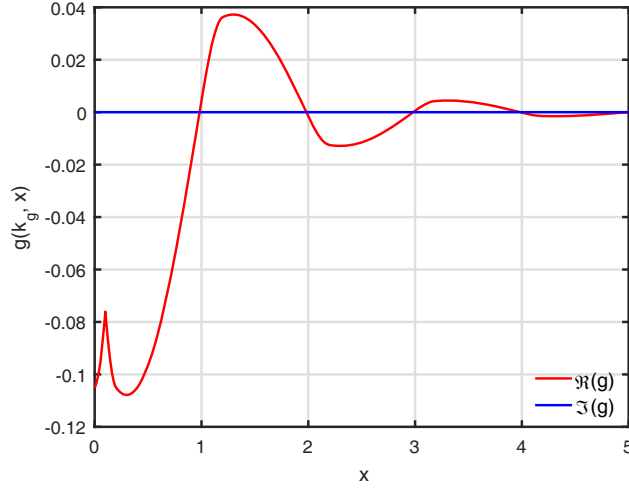
**Figure 8.** The midband point source Green's function for $0 \le x \le 5$, $x' = 0.1$ and $k_g = 2.3$.
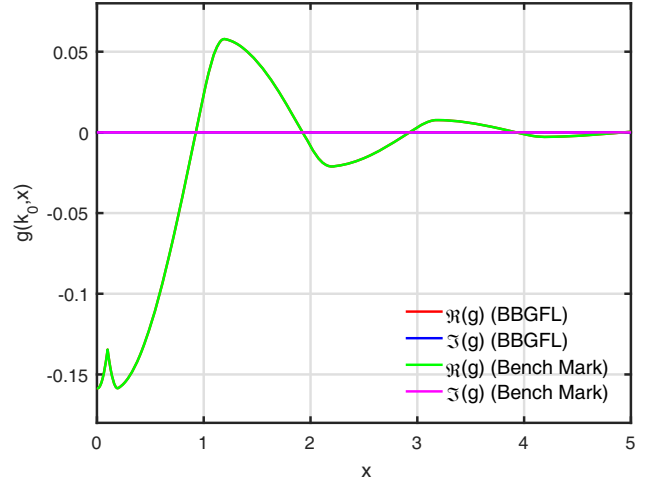
**Figure 9.** Point source Green's function for $k_0 = 2$.

extraction

$$e^{ik_i(x-x')} \sum_{\gamma} \left[ \frac{1}{k_{0\gamma}^2(k_i) - [k_0(1+i\epsilon)]^2} - \frac{1}{k_{0\gamma}^2(k_i) - k_g^2} \right] u_{1\gamma}^{S*}(k_i, x') u_{j\gamma}^{S}(k_i, x) \tag{129}$$

and the term with the extraction

$$e^{ik_i(x-x')} \left\{ \sum_{\gamma} \left[ \frac{1}{k_{0\gamma}^2(k_i) - [k_0(1+i\epsilon)]^2} - \frac{1}{k_{0\gamma}^2(k_i) - k_g^2} \right] u_{1\gamma}^{S*}(k_i, x') u_{j\gamma}^{S}(k_i, x) \right.$$

$$\left. - \left[ \frac{\text{Resid}_j(k_{i0}, x, x')}{k_i - k_{i0} - \dfrac{k_0 i\epsilon}{k_0^{(m)'}(k_{i0})}} + \frac{\text{Resid}(-k_{i0}, x, x')}{k_i + k_{i0} + \dfrac{k_0 i\epsilon}{k_0^{(m)'}(k_{i0})}} \right] \right\} \tag{130}$$

In Figures 10(a) and 10(b), we plot respectively the two terms in the first Brillouin zone with $x = 0.07$. The effects of the pole are shown in Figure 10(a). In Figure 10(b), after the poles are subtracted, the integrand is smooth in the first Brillouin zone. The smoothness of the integrand facilitates the integration of $I_1$ over the FBZ.

In Figures 11(a) and 11(b), we plot the point source Green's functions respectively for $0 \le x \le 1$ and $0 \le x \le 50$. The BBGFL solution and the benchmark solutions completely overlap.

### 4.4.3. Passband Very Close to Band Edge $k_0 = 1.511473682$

This case corresponds to $\beta_0 = 0.49$ and $k_{i0} = 3.0787608$. The first and second order derivatives are, respectively, $k_0^{(m)'}(k_{i0}) = 0.039935$ and $k_0^{(m)''}(k_{i0}) = -0.633387$. This is close to the band edge. Because it is close to the band edge, the first order derivative is small. We use the modal approach with second order extraction. The integral $I_1$ is performed numerically over the FBZ.

We choose the artificial loss to be $\epsilon = 2 \times 10^{-5}$. For this case, the two poles are at $k_{P1} = 3.0787562 + i0.0007569$ and $k_{P2} = 3.2048652 - i0.0007569$. The integrand, without the extraction, has the term

$$\sum_{\gamma} \left[ \frac{1}{k_{0\gamma}^2(k_i) - [k_0(1+i\epsilon)]^2} - \frac{1}{k_{0\gamma}^2(k_i) - k_g^2} \right] u_{1\gamma}^{S*}(k_i, x') u_{j\gamma}^{S}(k_i, x) \tag{131}$$
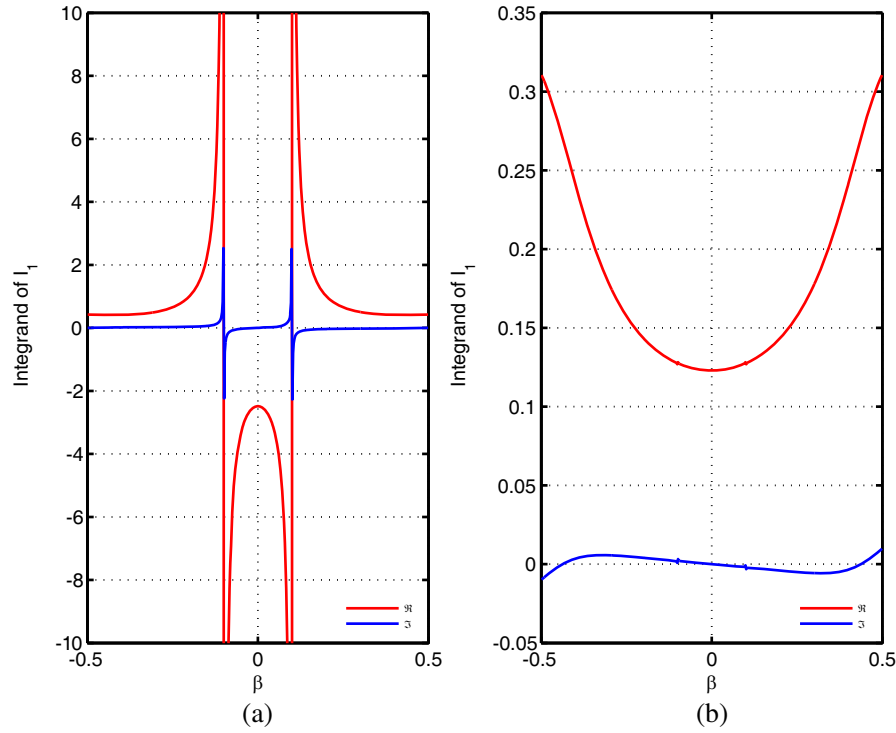
**Figure 10.** The effects of poles on the integrand of $I_1$ in the FBZ. (a) Before the poles are subtracted, Eq. (129), and (b) after the poles are subtracted, Eq. (130).
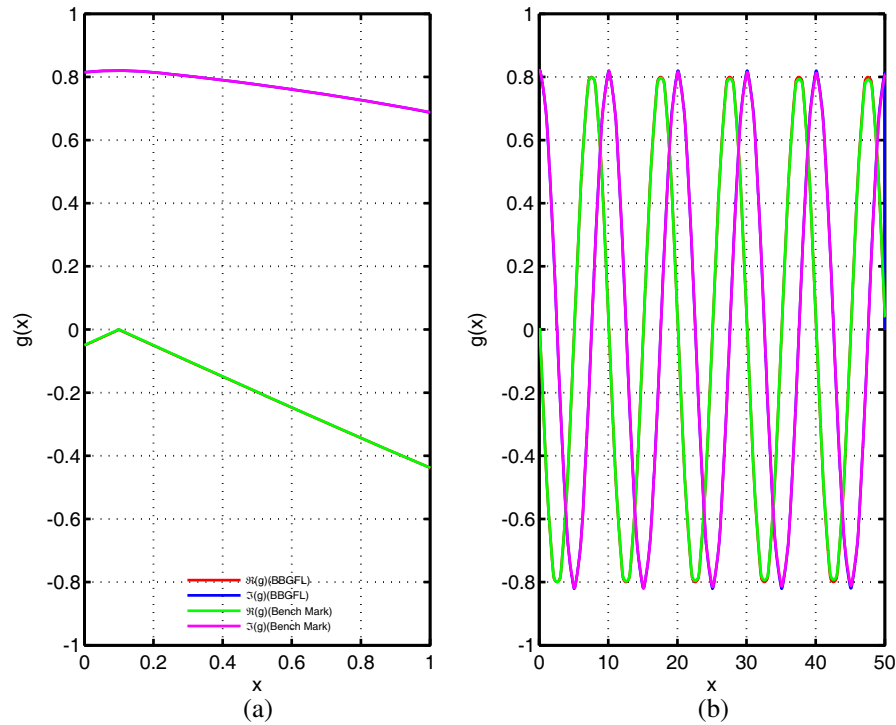


**Figure 11.** The point source Green's functions for $k_0 = 0.38958$ over (a) $0 \leq x \leq 1$ and (b) $0 \leq x \leq 50$. The BBGFL solutions are compared with the bench mark results.
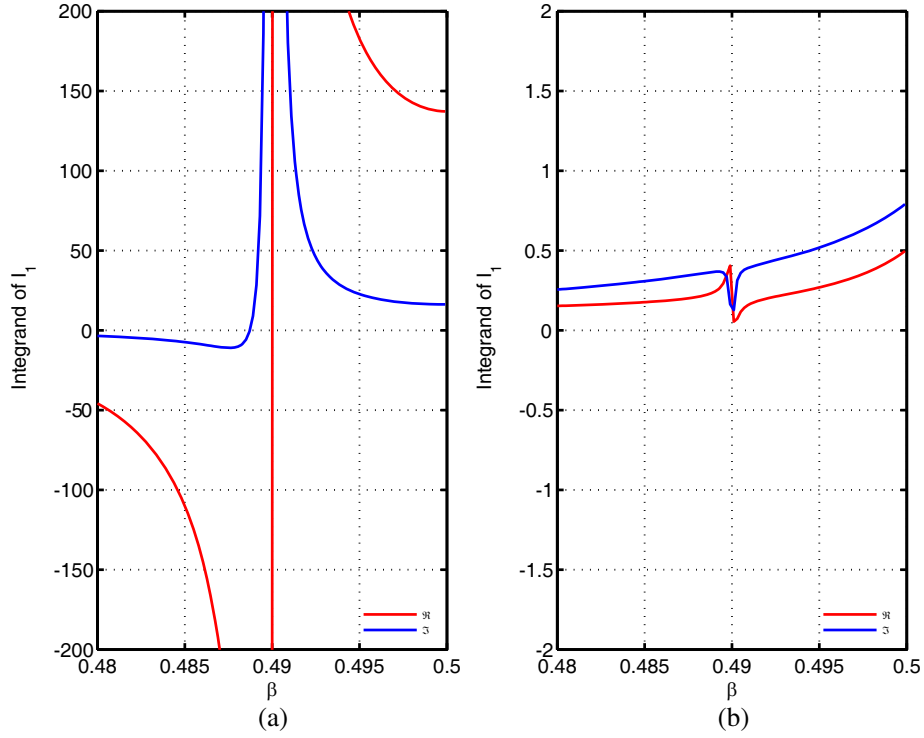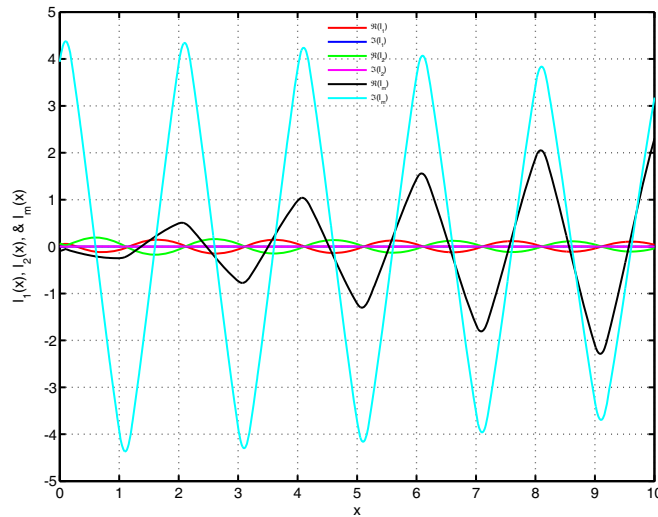
**Figure 12.** The effects of poles on the integrand in the FBZ. (a) Before the poles are subtracted, and (b) after the poles are subtracted.



**Figure 13.** Integrals $I_1$, $I_2$, and $I_m$.

With the second order pole extraction, the term becomes

$$
\sum_{\gamma} \left[ \frac{1}{k_{0\gamma}^2 (k_i) - [k_0 (1 + i\epsilon)]^2} - \frac{1}{k_{0\gamma}^2 (k_i) - k_g^2} \right] u_{1\gamma}^{S*} (k_i, x') u_{j\gamma}^{S} (k_i, x)
$$

$$
- \frac{2k_m' (k_{i0})}{k_m'' (k_{i0})} \left\{ \frac{\mathrm{Resid}_j (k_{i0}, x, x')}{(k_i - k_{P1}) (k_i - k_{P2})} + \frac{[\mathrm{Resid} (k_{i0}, x, x')]^*}{(k_i + k_{P1}) (k_i + k_{P2})} \right\} \tag{132}
$$

In Figures 12(a) and 12(b), we plot respectively the two terms in the first Brillouin zone for
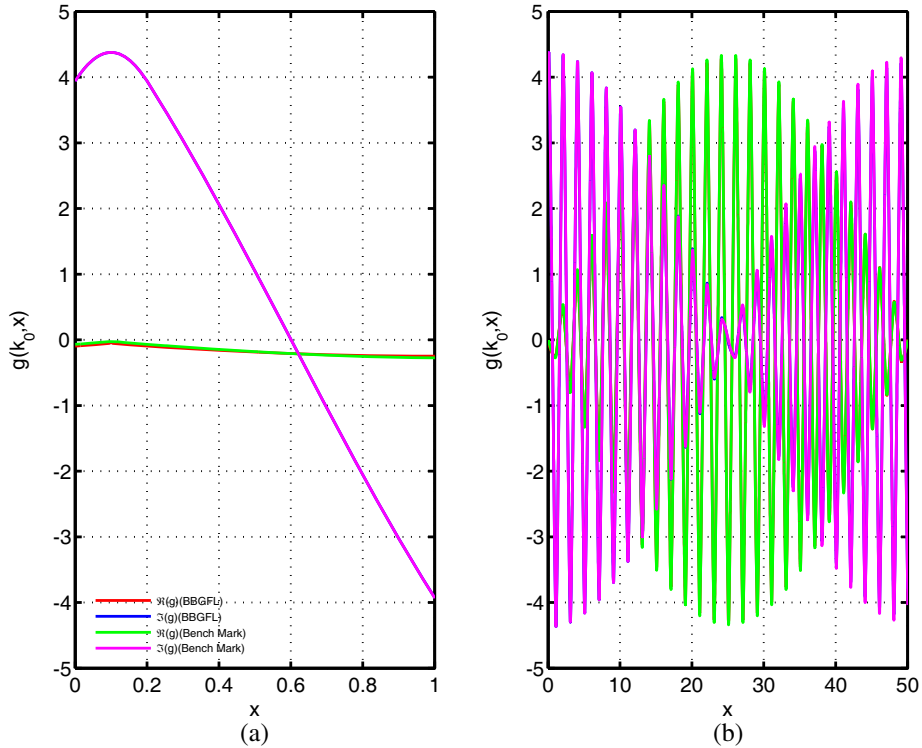
**Figure 14.** Point source Green's function for $k_0 = 1.511473682$.

the range $0.48 < \beta < 0.5$ with $x = 0.07$. The effects of the two poles $k_{P1}$ and $k_{P2}$ are shown in Figure 12(a). In Figure 12(b), after the second order extraction, the integrand is much smoother. Note that the vertical scales between Figures 12(a) and 12(b) are 100 times different. The smoothness of the integrand facilitates the integration of $I_1$ over the FBZ.

The case of $k_0 = 1.511473682$ is corresponding to $\beta_0 = 0.49$, which is very close to the band edge. We use the modal approach with the second order extraction. The integral $I_1$, with the second order pole extractions, is performed numerically over the FBZ. We choose the artificial loss with $k_0 = 1.511473682(1 + i\epsilon)$ where $\epsilon = 2 \times 10^{-5}$. In Figure 13, we plot integrals $I_1$, $I_2$, and $I_m$. The results show the relative contributions to the point source Green's function.

In Figures 14(a) and 14(b), we plot the point source Green's functions, respectively, for $0 \leq x \leq 1$ and $0 \leq x \leq 50$. The BBGFL solution and the benchmark solutions are in good agreement with each other.

## 5. CONCLUSIONS

In this paper we calculate the broadband Green's function of a single point source in a one-dimensional infinite periodic lossless medium using the method of BBGFL. Several improvements are made on the BBGFL method. In particular, the BBGFL of passband and near the band edge are calculated with a modal method. The BBGFL computed solutions are in good agreement with those of scattering solutions for stopband, passband, and close to the band edge.

The point source Green's functions are system responses of wave phenomena in photonic devices with periodic structures. Solutions of dielectric periodic structures, in the past, have been limited to photonic bands without rigorous studies of band field functions. The Green's function, in terms of bands, can give a band interpretation of the physical behavior that facilitates the design of photonic devices based on resonant electromagnetic modes [26]. Since band fields are independent of frequency, the Green's functions are readily calculated over a broad range of frequencies.

The single point source Green's functions in an "infinite" periodic structure is the physical response

of a single point source. It can be used to formulate integral equations for problems of finite periodic structures, impurities, etc. [12, 16]. The analogy is the free space Green's function which is for "infinite" homogeneous medium, yet one uses it to formulate integral equations for scatterers of finite size showing that "infinite" can be used for "finite". For example, in scattering from finite array of periodic scatterers [12], we formulate dual surface integral equation with the surface being an artificial boundary enclosing the finite array. When approaching the boundary from outside, the free space Green's function of infinite homogenous medium is used. When approaching the boundary from inside, the single point source Green's function of infinite periodic structure is used. In the problem of an impurity in a periodic structure, we formulate dual surface integral equation with the surface being an artificial boundary enclosing the impurity [16]. When approaching the boundary from inside, the free space Green's function of infinite homogenous medium is used. When approaching the boundary from outside, the single point source Green's function of infinite periodic structure is used.

This paper is going back from 2D/3D to 1D to clarify and improve key points in the BBGFL procedure. The improvements are accurate solutions for the hybrid combination of boundary terms and plane wave summations, accurate normalization, a single low wavenumber extraction, first and second order modal extractions in integration over the first Brillouin zone. In addition, the results of 1D case are completely validated by using 200,000 layers in the brute force scattering method. The validation will be difficult for the brute force methods in 2D/3D.

## APPENDIX A. DERIVATION OF EQS. (14) AND (15)

In this Appendix, we derive Eqs. (14) and (15). The free space Green's function of medium 2 is $g_2(k_0, x, x')$ which satisfies the following wave equation.

$$\frac{d^2 g_2 (k_0, x, x')}{dx^2} + k_0^2 \frac{\varepsilon_2}{\varepsilon_0} g_2 (k_0, x, x') = -\delta (x - x') \tag{A1}$$

We then have

$$\frac{d}{dx} \left[ \psi_2 (x) \frac{dg_2 (k_0, x, x')}{dx} - g_2 (k_0, x, x') \frac{d\psi_2 (x)}{dx} \right] = -\psi_2 (x) \delta (x - x')$$

Next, we perform summation and integration, $\sum_n \int_{na+b}^{(n+1)a} dx$, on the above equation.

$$\sum_n \int_{na+b}^{(n+1)a} dx \frac{d}{dx} \left[ \psi_2(x) \frac{dg_2(k_0, x, x')}{dx} - g_2 (k_0, x, x') \frac{d\psi_2(x)}{dx} \right] = -\sum_n \int_{na+b}^{(n+1)a} dx \psi_2(x) \delta(x - x') \tag{A2}$$

Let $x = na + x''$, using the Bloch condition $\psi_2(na + x'') = e^{ik_i na} \psi_2(x'')$ and changing the variable $x'' \to x$, Eq. (A2) can be rewritten as

$$\sum_n \left[ e^{ik_i na} \psi_2 (x) \frac{dg_2 (k_0, na + x, x')}{dx} - g_2 (k_0, na + x, x') \frac{d\psi_2 (x)}{dx} e^{ik_i na} \right]_{x=b}^{x=a}$$

$$= -\sum_n \int_b^a dx e^{ik_i na} \psi_2 (x) \delta (na + x - x')$$

Use the symmetry of free space Green's function $g_2$ and interchange arguments in the free space Green's function, the above equation becomes

$$\sum_n \left[ e^{ik_i na} \psi_2 (x) \frac{dg_2 (k_0, x', na + x)}{dx} - g_2 (k_0, x', na + x) \frac{d\psi_2 (x)}{dx} e^{ik_i na} \right]_{x=b}^{x=a} \tag{A3}$$

$$= \begin{cases} 0 & \text{for } 0 < x < b \\ -\psi_2 (x') & \text{for } b < x < a \end{cases}$$

The periodic Green's function $g_{2P}(k_0, x, x')$ is defined by adding $na$ to the second argument of $g_2$, followed by multiplication of $e^{ik_i na}$ and summation over $n$.

$$g_{2P} (k_0, x, x') = \sum_n e^{ik_i na} g_2 (k_0, x, na + x') \tag{A4}$$

Then we have

$$\left[\psi_2(x)\frac{dg_{2P}(k_0,x',x)}{dx} - g_{2P}(k_0,x',x)\frac{d\psi_2(x)}{dx}\right]_{x=b}^{x=a} = \begin{cases} 0 & \text{for } 0 < x < b \\ -\psi_2(x') & \text{for } b < x < a \end{cases} \tag{A5}$$

We switch $x' \Longleftrightarrow x$ and use the following properties to change the limit of $x'$ from $a$ to 0.

$$\psi_2(a) = e^{ik_ia}\psi_2(0) = e^{ik_ia}\psi_1(0) \tag{A6a}$$

$$g_{2P}(k_0,x,a) = e^{-ik_ia}g_{2P}(k_0,x,0) \tag{A6b}$$

## APPENDIX B. BBGFL FOR BAND SOLUTION DETAILS

In Section 2, the following matrices are used. In matrix $\bar{\bar{A}}$, the low wavenumber $\bar{\bar{R}}_1(k_{0L})$ and $\bar{\bar{R}}_2(k_{0L})$ are $2 \times M$ matrices with, respectively,

$$\bar{\bar{R}}_{1,\alpha}^{(j)}(k_{0L}) = R_\alpha^{(j)}(k_{0L},0) \tag{B1a}$$

$$\bar{\bar{R}}_{2,\alpha}^{(j)}(k_{0L}) = R_\alpha^{(j)}(k_{0L},b) \tag{B1b}$$

The matrices $\bar{\bar{Q}}_1(k_{0L})$ and $\bar{\bar{Q}}_2(k_{0L})$ are of dimension $M \times 2$ with, respectively,

$$\bar{\bar{Q}}_{\alpha,1}^{(j)}(k_{0L}) = Q_\alpha^{(j)}(k_{0L},0) \tag{B2a}$$

$$\bar{\bar{Q}}_{\alpha,2}^{(j)}(k_{0L}) = Q_\alpha^{(j)}(k_{0L},b) \tag{B2b}$$

where

$$Q_\alpha^{(j)}(k_{0L},x) = (-ik_{i\alpha})R_\alpha^{(j)}(k_{0L},-x)$$

Also, the matrices $\bar{\bar{T}}_1(k_{0L})$ and $\bar{\bar{T}}_2(k_{0L})$ are of dimension $M \times 2$ with, respectively,

$$\bar{\bar{T}}_{\alpha,1}^{(j)}(k_{0L}) = T_\alpha^{(j)}(k_{0L},0) \tag{B3a}$$

$$\bar{\bar{T}}_{\alpha,2}^{(j)}(k_{0L}) = T_\alpha^{(j)}(k_{0L},b) \tag{B3b}$$

where

$$T_\alpha^{(j)}(k_{0L},x) = R_\alpha^{(j)}(k_{0L},-x)$$

The matrices $\bar{\bar{D}}_1$, $\bar{\bar{D}}_2$, $\bar{\bar{W}}_1$ and $\bar{\bar{W}}_2$ are diagonal of size $M$ with, respectively,

$$\bar{\bar{D}}_{\alpha,\beta}^{(j)} = D_\alpha^{(j)}\delta_{\alpha\beta} \tag{B4}$$

and

$$\bar{\bar{W}}_{\alpha,\beta}^{(j)} = W_\alpha^{(j)}\delta_{\alpha\beta} \tag{B5}$$

## REFERENCES

1. Tai, C. T., *Dyadic Green's Function in Electromagnetic Theory*, International Textbook, Scranton, PA, 1975.
2. Felsen, L. P. and N. Marcuvitz, *Radiation and Scattering of Waves*, Prentice Hall, Englewood Cliffs, NJ, 1973.
3. Kong, J. A., *Electromagnetic Wave Theory*, 2nd Edition, John Wiley & Sons, New York, 1990.
4. Tsang, L., J. A. Kong, and R. T. Shin, *Theory of Microwave Remote Sensing*, Wiley-Interscience, New York, 1985.
5. Chew, W. C., *Waves and Fields in Inhomogeneous Media*, IEEE Press, New York, 1995.
6. Tsang, L. and S. Huang, "Broadband Green's function with low wavenumber extraction for arbitrary shaped waveguide and applications to modeling of vias in finite power/ground plane," *Progress In Electromagnetics Research*, Vol. 152, 105–125, 2015.

7. Tsang, L., "Broadband calculations of band diagrams in periodic structures using the broadband Green's function with low wavenumber extraction (BBGFL)," *Progress In Electromagnetics Research*, Vol. 153, 57–68, 2015.

8. Huang, S. and L. Tsang, "Fast electromagnetic analysis of emissions from printed circuit board using broadband Green's function method," *IEEE Trans. Electromagn. Compat.*, Vol. 58, 1642–1652, 2016.

9. Tsang, L. and S. Tan, "Calculations of band diagrams and low frequency dispersion relations of 2D periodic dielectric scatterers using broadband Green's function with low wavenumber extraction (BBGFL)," *Opt. Express*, Vol. 24, 945–965, 2016.

10. Liao, T.-H., K.-H. Ding, and L. Tsang, "High order extractions of broadband Green's function with low wavenumber extractions for arbitrary shaped waveguide," *Progress In Electromagnetics Research*, Vol. 158, 7–20, 2017.

11. Tan, S. and L. Tsang, "Green's functions, including scatterers, for photonic crystals and metamaterials," *J. Opt. Soc. Am. B*, Vol. 34, 1450–1458, 2017.

12. Tan, S. and L. Tsang, "Scattering of waves by a half-space of periodic scatterers using broadband Green's function," *Opt. Lett.*, Vol. 42, 4667–4670, 2017.

13. Tsang, L. W. and S. Huang, "Full wave modeling and simulations of the waveguide behavior of printed circuit boards using a broadband Green's function technique," U.S. Patent 9,946,825, issued April 17, 2018.

14. Tsang, L., K.-H. Ding, T.-H. Liao, and S. Huang, "Modeling of scattering in arbitrary-shape waveguide using broadband Green's function with higher order low wavenumber extractions," *IEEE Trans. Electromagn. Compat.*, Vol. 60, 16–25, 2018.

15. Kwek, W., L. Tsang, K.-H. Ding, and T.-H. Liao, "Broadband Green's function with higher order extractions for arbitrary shaped waveguide obeying Neumann boundary conditions," *2018 IEEE International Symposium on Electromagnetic Compatibility and 2018 IEEE Asia-Pacific Symposium on Electromagnetic Compatibility (EMC/APEMC)*, 72–75, IEEE, 2018.

16. Tan, S. and L. Tsang, "Effects of localized defects/sources in a periodic lattice using Green's function of periodic scatterers," *2108 IEEE International Symposium on Antennas and Propagation and USNC-URSI Radio Science Meeting*, Boston, MA, USA.

17. Tsang, L. W. and S. Tan, "Full wave simulations of photonic crystals and metamaterials using the broadband Ggreen's functions," U.S. Patent Application 15/798,148, filed May 3, 2018.

18. Zhang, W., C. T. Chan, and P. Sheng, "Multiple scattering theory and its application to photonic band gap systems consisting of coated spherers," *Opt. Express*, Vol. 8, 203–208, 2001.

19. Ergül, E., T. Malas, and L. Gürel, "Analysis of dielectric photonic-crystal problems with MLFMA and Schur-complement preconditioners," *J. Lightw. Technol.*, Vol. 29, 888–897, 2011.

20. Yasumoto, K., *Electromagnetic Theory and Applications for Photonic Crystals*, CRC Press, 2006.

21. Yariv, A. and P. Yeh, *Optical Waves in Crystals*, John Wiley, New Jersey, 2003.

22. Joannopoulos, J. D., S. G. Johnson, J. N. Winn, and R. D. Meade, *Photonic Crystals: Modeling the Flow of Light*, Princeton University, 2011.

23. Luo, M. and Q. H. Liu, "Spectral element method for band structures of three-dimensional anisotropic photonic crystals," *Phys. Rev. E*, Vol. 80, 056702, 2009.

24. Johnson, S. G. and J. D. Joannopoulos, "Block-iterative frequency-domain methods for Maxwell's equations in a planewave basis," *Opt. Express*, Vol. 8, 173–190, 2001.

25. Ashcroft, N. W. and N. D. Mermin, *Solid State Physics*, Holt, Rinehart and Winston, New York, 1976.

26. Sakoda, K., *Optical Properties of Photonic Crystals*, Springer-Verlag, 2001.